Reconciling Modal and Time Domain Techniques in Photonic Simulation

by

Christos D. Samolis

S.B. Electrical Science and Engineering
Massachusetts Institute of Technology (2012)

Submitted to the Department of Electrical Engineering and Computer Science
in Partial Fulfillment of the Requirements for the Degree of

Master of Engineering in Electrical Engineering and Computer Science
at the
Massachusetts Institute of Technology

May 2015
[February 2016]

Signature redacted

Signature of Author: .....
Department of Electrical Engineering and Computer Science
May 22, 2015

Signature redacted

Certified by: ..
.....
Luca Daniel
Associate Professor
Thesis Supervisor

Signature redacted

Accepted by: .....
.....
Albert R. Meyer
Hitachi America Professor of Computer Science
Chairman, Masters of Engineering Thesis Committee

This page is intentionally left blank.

Reconciling Modal and Time Domain Techniques in Photonic Simulation

by

Christos D. Samolis

Submitted to the Department of Electrical Engineering and Computer Science on May 22, 2015 in Partial Fulfillment of the Requirements for the Degree of Master of Engineering in Electrical Engineering and Computer Science

Abstract

Three dimensional Finite Difference Time Domain (3D-FDTD) simulation serves as the indisputable gold standard for device design and verification in silicon photonics. However, 3D-FDTD is prohibitively expensive for large devices let alone cascaded systems, leading to the pursuit of a diversified simulation toolkit to acquire the full device response or combined device (cascade or parallel) response. A modular approach is followed subsequently. For analyzing silicon photonics at the systems level, transfer matrices in the modal/frequency domain are ubiquitously used. These matrices encapsulate the frequency response as well as the coupling coefficients between the various optical eigenmodes across all device ports. In this thesis we formulate and explore the performance of a fast, memory efficient stand-alone FDTD based algorithm that uses transfer matrices within the simulation window for the optical characterization of adiabatic mode-evolution devices. This class of adiabatic devices is vital to silicon photonics systems thanks to their broadband nature and reliable performance under fabrication induced perturbations and parameter variation.

In our approach, the simulation domain is divided into blocks which can be simulated independently in the time domain, and then combined using modal transfer matrices. It is critical that we can match the accuracy of a 3D-FDTD simulation for a base class of devices and make an argument that time domain and modal techniques can be perfectly reconciled in a simulation environment where these devices appear and play a significant role. This environment might be targeting a particular device or even an entire section of the chip. When compared to pure 3D-FDTD this approach proves auspicious from a computational standpoint as it yields, in the limit of large devices, an asymptotic linear speedup when the blocks are simulated sequentially, and can further yield a quadratic speedup when an extra level of parallelization is employed.

Thesis Supervisor: Luca Daniel

Title: Professor

This page is intentionally left blank.

Acknowledgments

I would especially like to thank my thesis supervisor Luca Daniel for all his support and encouragement. I have been fortunate to have had the privilege to interact with him in a variety of settings whether in research or teaching courses and he has repeatedly proven to be passionate and outstanding at what he does making him an immensely talented mentor for both academics and life.

I would also like to thank Mike Watts, Ami Yaacobi, Cheryl Sorace Agaskar, Michele Moresco, David Bernard Cole, Zhan Su, Sasha Biberman, Anna Baldycheva, Erman Timurdogan, Ehsan Shah Hosseini, Jie Sun, Patrick Callahan, Katia Shtyrkova, Ben Moss and Stevan Urosevic for their warm advice, immensely helpful technical discussions and the provision of useful supplemental materials. Each of these individuals has given me their *time*, each in his/her own way. Since time is the single currency of the universe, that is perhaps the most laconic way to thank them and lumps a lot more value than a lengthier elaboration would.

I would like to thank my family and in particular my parents, Patricia and Dimitrios, to whom I dedicate this thesis. It's very difficult for me to put anything into words that would accurately portray all they have done for me, ever since I was a little kid, but they know and that suffices.

Lastly, I would like to thank God.

ΕΝ ΟΙΔΑ ΟΤΙ ΟΥΔΕΝ ΟΙΔΑ

ΣΩΚΡΑΤΗΣ

This page is intentionally left blank.

Table of Contents

Title Page / Abstract 3

Acknowledgments 5

1. Introduction 10

1.1 From Fiber Optics to VLSI Silicon Photonics 10

1.2 A Diversified Simulation Toolkit for Systems-Level Photonics 16

1.3 Problem Statement 19

1.4 Original Contribution and Thesis Objectives 21

2. Background on the Finite Difference Time Domain Technique 27

2.1 The Yee Lattice 27

2.2 Computational Complexity of 3D-FDTD 33

3. Background on Eigenmode Expansion and Transfer Matrices 37

3.1 Modal Solutions to Dielectric Waveguide Problems 37

3.2 A Vector Space Picture and Transfer Matrices 45

4. Background on FDTD Speedup Approaches **48**

4.1 The Segmented Finite Difference Time Domain (FDTD) Method 48

4.2 Sparse FDTD and Pulse Tracking Approaches 49

5. A Hybrid FDTD-Transfer Matrix Method: (TM-FDTD) **52**

5.1 TM-FDTD Technique Formalization 52

5.2 Computational Analysis and Experimental Verification 58

5.3 Implementation for a Polarization Rotator 60

6. Conclusions **64**

Bibliography **67**

This page is intentionally left blank.

Chapter 1

Introduction

1.1 From Fiber Optics to VLSI Silicon Photonics

Very-large-scale integrated (VLSI) silicon photonics is ripe for commercial development. In particular, CMOS compatible VLSI photonics seems to be the inevitable solution to the increasing demand for processing record high bandwidth in both Datacom and Telecom. With Moore's law coming to a halt, we are no longer able to crank the knob of transistors/area to satisfy this data processing demand. Silicon photonics innovation is of particular relevance to large data center farms such as those owned by Google. In Telecomm, silicon photonics can help realize optical flow switching architectures that directly route large bandwidth in the optical domain combined with direct optical reception at the end nodes [1].

Let's consider a sample data flow on a future hybrid computer chip. In our hypothetical scenario, you tap IR light coming from a port on the wall, and through some fiber connector, that light couples into a designated optical layer on a hybrid motherboard and eventually couples onto a packaged chip. That packaged chip may have the photonics on one side, and the CMOS on the opposite side and the layers may communicate through 3D vias [2]. They could also be monolithically integrated in a two dimensional fashion and be located on the same face of the chip. The coupled light might contain multiple polarizations.

Perhaps it undergoes polarization splitting sending a TE (transverse electric) or horizontally polarized component to a TE-designated part of the chip, and a TM (transverse magnetic) or vertically polarized component to a TM-designated part of the chip [3]. Or perhaps the TM component gets rotated to TE to be processed on an exclusively TE processing sector [4]. The light that has coupled onto the chip may also contain multiple wavelength channels. An on-chip filter bank may separate those channels into separate waveguides each of which goes through a separate processing pathway.

Consider one channel. A wavelength insensitive switch matrix could route that signal to the right processing unit, or CPU core, as commanded by an electrical address signal. Perhaps the light is later converted to an electrical signal through a Germanium photo-detector [5], the electrical signal gets transferred over to the CMOS layer, some processing takes place, and then a laser on the photonics side sends a beam through an activated modulator. The optical modulation is realized based on electrical commands from the previous process whether thermo-optically (voltage → temperature → refractive index shift) or via carrier injection and depletion. This modulated beam then leaves to go to some other place on the chip, or maybe gets mixed with other wavelengths and collectively (as part of a grander WDM transceiver scheme) couples out of the chip into a fiber and goes back through the wall from which it came from. From there it could travel outbound through the metropolitan area network (MAN) to service your video streaming for instance. Alternatively, maybe it (along with other channels) gets split, weighted and emitted through an optical phased array, and received via an

antenna array or broadband vertical coupler on another chip in the same package after having propagated through a free space gap. From there it can undergo a similar journey. Prior to leaving the computer/node altogether, this hypothetical path that we've considered could undergo processing at multiple chips, coupling in and out and getting transported around via the optical layer in the motherboard.

Please note that the aforementioned ride is not to be taken literally as performing a specific function. It might indeed be purposeless to have that many nested levels of electrical to optical conversion or combination of vertical and side coupling across multiple chips. It's merely an illustrative example that attempts to lump as many steps as possible to completely cover and convey the functionality of the photonics device kit. It is meant to be descriptive of the ways in which photonics and electronics can be reconciled in future architectures, illustrating the seamlessness of manufacturing and design, and the crossing of boundaries from one domain to the other [6]. These innovations are not merely technological in nature and impact, but could ultimately lead to a new cultural era, one of streaming Terabytes per second on your home computer and being able to take that for granted.

Interestingly enough the technology for the development of silicon photonics is not in essence new to the scene. For decades optical fibers (Charles Kao Nobel Prize 2009) empowered by erbium doped amplifiers have been responsible for weaving together the World Wide Web. This is due to a miraculous coincidence

of the low attenuation (<0.3 dB/km) frequency range in optical fibers overlapping with the gain region in erbium doped fiber (fiber that has erbium ions implanted in the core). The combination of these two accidental and empowering factors allows for long distance information-preserving optical propagation. Absent the military priorities of the Cold War and the fact that Big Data could have provided no advantages to solving a pertinent problem of the time such as inertial navigation, silicon photonics development could have taken off much sooner. But today it's a different game altogether.

Admittedly the first decade of the 21st century has left its mark both in terms of the ubiquitous appearance and importance of Big Data (demand) but also in terms of significant milestones for the direct on-chip processing of light (supply/solution) that gets transported through optical fibers [7], [8], [9], [10]. This has led to financial incentives and initiatives in favor of silicon photonics development. Optical fibers that make up the long haul backbone of the internet will increasingly perforate networking at all levels. With the diminishing necessity for optical to electrical conversion, and thanks to the compact footprint of integrated devices (~ μm^2 for photonics) and (~ nm^2 for CMOS) it will be possible to create complex hybrid electronic optical systems that process Terabytes of data every second on the same silicon chips that have allowed the exponential scaling of traditional transistors with high density integration [11].

Most importantly, this can be accomplished using similar (or at least compatible) fabrication processes. The latter is key to the commercial promise and feasibility

of silicon photonics as many decades of development and investment in microelectronics have set inertial standards in a nearly 400 billion dollar industry and an even greater valued technology enabler. CMOS compatibility not only dictates the design and development pathway but is also of high relevance for the proper placement of the work presented in this thesis.

A large-scale hybrid electronic-photonic system requires a massive and complex design effort [12] and it would be great if existing practices applicable to this design process could seamlessly be bridged from CMOS, and directly implemented on the photonics side. In CMOS, software such as LT-spice and Cadence along with backend coding in an abstraction/modeling oriented language such as Verilog are widely used to model complex systems using transfer matrices. Commercial packages are already attempting to establish the same culture in photonics for designing reliable large-scale systems. So long as silicon photonics and CMOS are married, this amplifies the high relevance and popularity of transfer matrices.

But this statement requires another level of context to be fully justified, the reality that photonics and CMOS will never get a divorce. Something that gets underappreciated or all out underestimated in dinosaur industries is the level of disruption that can take place when a new technology simply outperforms the status quo in every possible way including performance, power consumption (which directly translates to usage cost), and production cost. The dinosaur

industry tends to cling to inertial hope such as the tear down cost of changing the infrastructure or the industry's established popularity and legacy.

But eventually supply and demand will lead to an extinction level event for any outdated technology no matter how ubiquitously well-established it might be. The tear down cost does not factor into this because that is only temporary and cannot compare to the long-term economic advantages which set the gradient direction. If we could dispense with electronics all together then protocols, development processes, and expensive multi-billion dollar foundries would collectively be annihilated by a tsunami of optical innovation. The Internet Protocol is a great example of a seemingly deified immobile boulder that in the future might very well give way to new protocols to best handle Optical Flow Switching and other disruptive optical network architectures [1]. But this is not at all the case with CMOS. Silicon photonics is not the tsunami that all-optical computing failed to be, and CMOS microelectronics is most likely here to stay for good [13].

First off, silicon photonics is not optical computing, in the sense that all control signals are and *need* to be realized electronically. The energy required to activate an optical transistor by a photon exceeds that of electron activation making all-optical computing an unrealistic scheme. Another major obstacle that has led to the decline of the excitement yielded by all-optical computing in the 80s is that virtually no significant progress has been made in using the output of an optical transistor to drive another transistor prohibiting cascaded system design.

Lastly, there is no optical equivalent to electronic random access memory that can be realized with storage longevity and a compact footprint. For these reasons, silicon photonics requires and will always require a co-existence with established CMOS. Although recent advances [14], [15] continue to expand the boundaries of physical insights in all-optical computing the practicality of such scheme is not widely accepted and remains a serious question.

The real advantage of silicon photonics is the ease of processing large bandwidth. For example, in multi-core processing systems data could be routed in the optical domain from core to core bypassing the memory bottleneck. Another dominating strength of these hybrid electronic-photonic systems is record low power consumption. The magical combination of ultra-high bandwidth and ultra-low power consumption (mainly in athermal design) make silicon photonics a very seductive business prospect for manufacturing giants (such as Intel or IBM) and startups alike.

1.2 A Diversified Simulation Toolkit for Systems-Level Photonics

The interaction of light with dielectric matter is modeled of course via Maxwell's equations. For the design of an arbitrary single micro-photonic element a 3D Finite Difference Time Domain simulation serves by default as the most rigorous and valid numerical simulation approach. This is because FDTD directly simulates Maxwell's equations in the time domain, and can therefore handle all electromagnetic phenomena naturally, limited only by the computational grid discretization level [16]. But the simulation of a computational volume on the

order of mm^3 is possible only with supercomputing capabilities, and even then not practical or worthwhile. For many devices in the silicon photonics toolkit modal sparseness might be a distinct feature that can be exploited.

In particular adiabatic mode-evolution devices by design contain a limited number of bound eigenmodes at every cross-section, with this fundamental mode number being preserved from beginning to end since the device is slowly varying [17]. Eigenmode expansion is especially favored in the community for this class of devices. Eigenmode expansion has stability issues however [18], and furthermore requires a relatively loose longitudinal discretization to be considerably faster than a carefully constructed FDTD simulation. But most importantly, the modal sparseness is assumed in advance by the designer to justify the use of this simulation technique. This creates an inescapable level of uncertainty. How can the designer be sure, especially for devices that exhibit a higher level of complexity such as a polarizing beam splitter [4], [19], that all the possible modes are taken into account or that the device remains adiabatic as he/she varies the longitudinal and transverse profile? It is therefore standard practice for an optimization sweep to be run using a fast modal technique like eigenmode expansion, and at the very least a full 3D-FDTD simulation is run at the end to confirm the final device [20].

In an SOI process all the device geometries need to be rectilinear due to constraints on fabrication capabilities. Unlike CMOS, rectilinear constraints on design are fundamentally limiting in photonics where engineering the shape of

the transverse profile can allow the design of arbitrarily sophisticated mode confinement and open up an entire region of design in "device space". However, it is currently the only reliable, affordable and scalable way to fabricate silicon waveguides, especially in CMOS compatible foundries. Therefore the width of the waveguides is set by the mask layer and the fabrication process, and is fixed. This makes it easy for photonics designers to frequently approximate 3D geometries with 2D geometries and run FDTD simulations in a 2D domain which is massively more efficient.

Other times an effective index approximation is used and a 2.5 dimensional FDTD simulation is conducted [21]. All of these approaches however that aim to reduce the dimensionality of FDTD are fundamentally inaccurate because they make simplifying approximations that deviate from reality. They create a fictitious device that resembles the actual one, so the simulation results will at best resemble or be in the right ballpark of the actual device response. It is worth clarifying that all lower dimensional versions of FDTD do not constitute "compressed algorithms", but rather simulate a physical reality that is different from the one that is actually desired. At the end it is again necessary to run a full 3D-FDTD simulation to confirm the device.

Other popular approaches especially suited to adiabatic devices are the time domain beam propagation method (BPM) which also has stability issues [22], [23], [24], [25], [26], and analytical techniques such as coupled mode theory (CMT) which can provide limited insights for simple devices [27].

1.3 Problem Statement

The trend in the community is to use scattering matrices for systems level characterization whose parameters may have been acquired via FDTD or other techniques. The take-away from this section of the thesis is that for the simulation of silicon photonics there is no single right answer. This is the current conclusion from the simulation state of the art [28], [29], [30]. Hybrid approaches and device specific speedups are constantly being sought for particular device classes that exhibit some exploitable characteristic such as periodicity. As a matter of fact, this is an excellent point to place the pursuit of FDTD algorithm design into an interesting scope summarized in Figure 1.

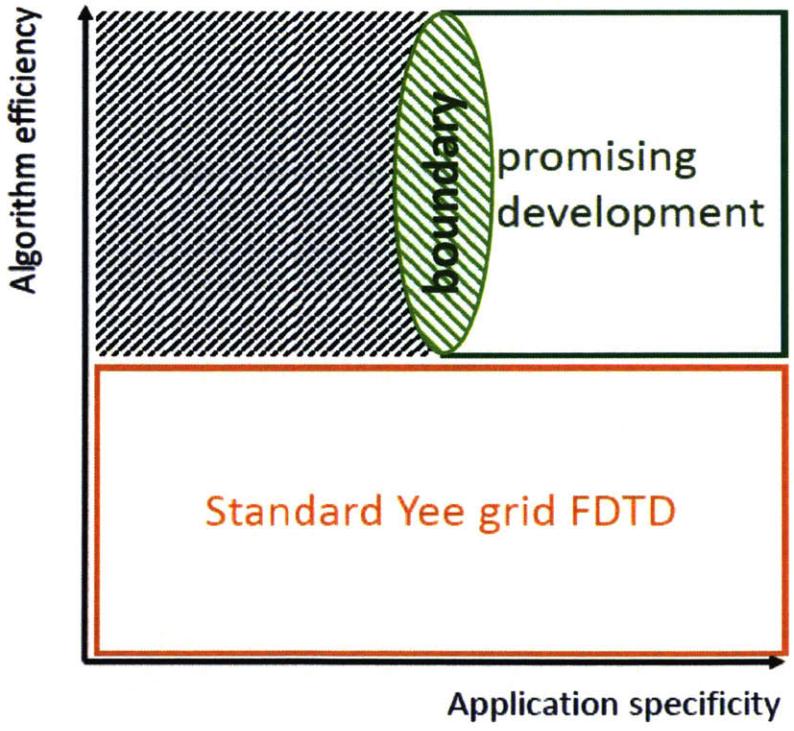

Figure 1: Value map for classifying current available solutions in FDTD, as well as the total open research space. Ideally we would like to push at the boundary of low specificity.

The novel insights behind the Yee grid have enabled an accurate discretization of Maxwell's curl equations and enabled the solution to a virtually unlimited spectrum of electromagnetic problems. The range of problems that can be decisively analyzed with FDTD is beyond impressive. These can range from electromagnetic pulse radiation propagation by a nuclear detonation in the ionosphere [31], to nanophotonic or even quantum optical simulation [32]. FDTD can handle scattering by dielectric spheres, nonlinear gain materials [33] and adiabatic mode evolution. It is immensely powerful and impactful precisely because it has such low application specificity. The tradeoff is that it's a rigorous, but an inherently resource heavy algorithm for an arbitrary problem of a certain computational size.

Extensive research has shown that this need not *always* be the case [20]. More often than not, a particular problem of interest exhibits several characteristics that can be leveraged to speed up accurate FDTD simulation for that particular problem, or better yet, a particular device class. The hybrid method developed in this thesis is attacking in the upper right corner of Figure 1 for the unique category of adiabatic mode-evolution devices, similar to a plethora of other propositions for different categories. It is interesting to note the lack of research and even the absence of a remote outline of a solution that attacks in the upper left quadrant of Figure 1. A new algorithm here, one that would potentially change the actual complexity class that FDTD falls under (instead of merely offering a speedup) would have seminal impact analogous to that of the Fast Fourier Transform (FFT) [34] which made all problems it was meant to tackle

able to be computed in $\mathcal{O}(n \log n)$ cputime from the previous $\mathcal{O}(n^2)$. This quadrant is currently dark, but by referring to it we can complete our topological value-map for FDTD which remains the most reliable of all simulation techniques in the photonics toolkit [35], [36].

1.4 Original Contribution and Thesis Objectives

The original contribution of this thesis is placed in the right scope taking into account the considerations of the previous section. In this thesis we specifically consider the class of adiabatic devices that are characterized by slow longitudinal dielectric variation as a case study and proof of concept for an efficient FDTD technique that uses transfer matrices within the simulation window. Transfer matrices are a vital ingredient to the recipe for the complete characterization of complex photonic systems aimed at VLSI.

These cascaded systems communicate with each other through single waveguides. On an SOI platform, patterned silicon waveguides serve as buses transporting many data channels under tight light confinement due to the high index contrast. However, the devices can still exhibit undesired optical crosstalk when combined together. This can undermine the overuse of scattering matrices especially if they have been acquired through diverse techniques (some modal, others time domain) and inclines one to simulate the entire chip in a consistent fashion. We will not go so far as to call this accumulation a numerically nonlinear process, but we do claim that there is greater confidence when as much real

estate of the chip as possible can be simulated in a pseudo-monolithic fashion. By a pseudo-monolithic fashion we refer to a consistent approach that makes it clear what accuracy tradeoffs there are (if any) at the unification joints. Of course, running an FDTD simulation for the entire chip is computationally beyond impractical if not all out impossible. Yet at the same time the desire is to run as much FDTD as possible. This is what needs to be reconciled and this is the culture that we need to bear in mind and is summarized in Figure 2.

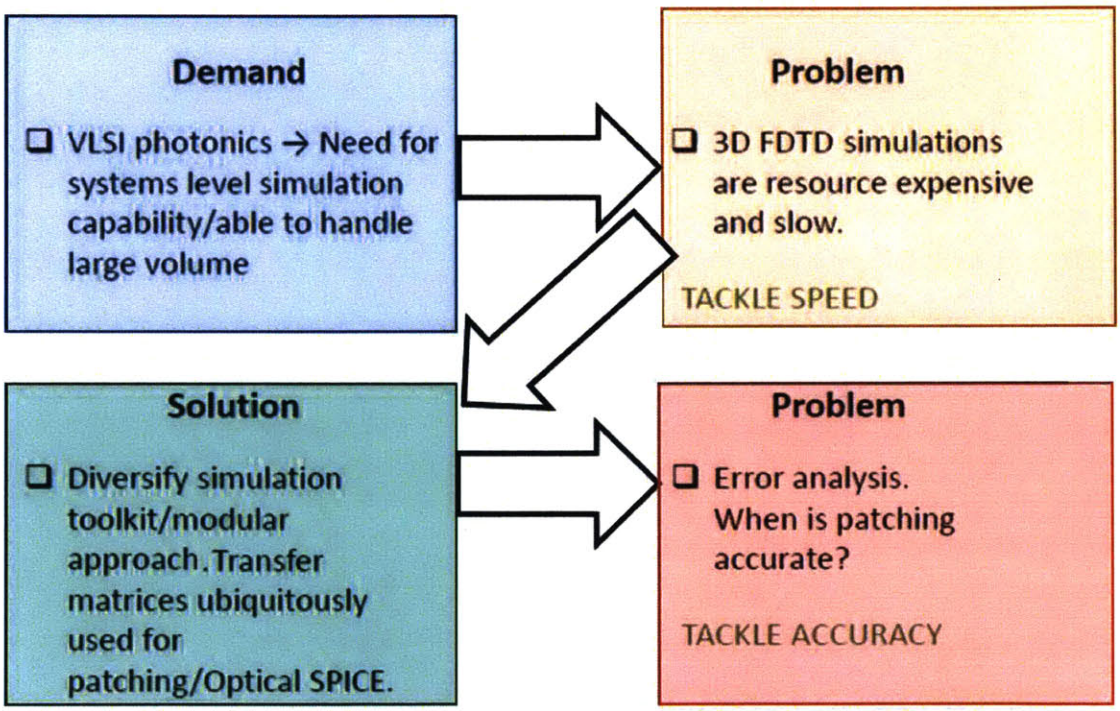

Figure 2: Summary of simulation landscape for silicon photonics systems.

The proposition of this thesis is a hybrid FDTD-Transfer Matrix method applicable to adiabatic photonic simulation. We propose a simulation technique that already employs multi-threaded FDTD with all the previously proposed levels of spatial parallelization, given the resources available. Under the assumption that the full transfer matrix is desired, an extra level of parallelization can be utilized in our technique (temporal parallelization) that is of a different nature than spatial parallelization, can be interleaved with it and further accelerate the simulation if more computational resources are available.

The simulation domain is divided into longitudinal blocks of equal dimensions each of which can be simulated separately in the time domain. Since the transverse plane remains fixed, this results in a linear speedup in the temporally sequential case (quadratic for the temporally parallelized) in the limit of large devices where computational overhead due to the calculation of eigenmodes and coupling coefficients can be neglected. This is perfectly adequate since the power of the technique lies in being able to simulate prohibitively large devices. For shorter devices, the method still yields a significant speedup but the variation might not vary linearly with the number of blocks. Similarly if the number of blocks is made exceedingly large relative to the computational domain size, overhead needs to be taken into account but this is more often than not a pathogenic parameter area.

Importantly, we show that the accuracy matches that of FDTD to two significant for a very short (~17 um) device, where the adiabatic limit is more likely to break

down. Thus, the accuracy will match 3D-FDTD for all identical devices of greater length. Due to limited computational resources exceedingly large devices were not simulated.

Chapter 1 of this thesis serves to introduce the field of silicon photonics and walk the reader through a minimally brief history from its inception to its upcoming relevance. It further aims to foster an appreciation of the difficulty in simulating large-scale photonic systems and how it behooves one to pursue a scalable and consistent technique that can bring together large sections of the chip at carefully chosen adiabatic junctions. Lastly, it hopes to leave the reader with the understanding that FDTD is the almighty king of any optical simulation and thus for any photonic simulation.

Chapter 2 of this thesis aims to introduce the basic algorithm behind FDTD that has made the technique applicable to discretizing Maxwell's equations. It does not cover every noteworthy aspect of FDTD, nor is it a mini-course on the subject but rather sets up the basic equations on the grid so that they can later be reconciled with the mode solver. It lastly mentions some of the advanced computing solutions that can be used for large scale problems that mainly involve maximizing the level of spatial parallelization.

Chapter 3 of this thesis begins by developing a brief theory of modal solutions to dielectric waveguide problems, and explains that the electric and magnetic field distributions in the transverse plane such as those recorded by the DFT monitors in a FDTD simulation lie in a vector space that can be resolved by the optical

eigenmodes. It thoroughly discusses the geometrical features that necessitate numerical solutions, and then discretizes the curl equations and Gauss's law to obtain those solutions via an eigenvalue problem. It introduces general transfer matrices and reconciles them with scattering matrices and eigenmodes. It also discusses some of the subtleties involved in calculating the coupling coefficients between eigenmodes, and the dot product relation in the aforementioned vector space.

Chapter 4 of this thesis performs a thorough comparison to the most distinct and noteworthy previous work that has attempted to speed up FDTD in ways similar and highly relevant to the techniques that this thesis builds on. It focuses on the segmented FDTD method and pulse tracking, both of which have lower application specificity and wider applicability than other more selective device specific speedups.

Chapter 5 proceeds to mathematically formalize the specific details of the hybrid FDTD-Transfer Matrix Method (TM-FDTD) using the foundations from chapters 2, 3 and 4. It discusses theoretical estimates on the computational performance and confirms the curves in simulation. Lastly, it presents complete results for the polarization rotator and demonstrates the equivalence to pure FDTD.

Chapter 6 summarizes the results and re-emphasizes the context of the thesis, but most importantly lays out significant directions for future work.

This page is intentionally left blank.

Chapter 2

Background on the Finite Difference Time Domain Technique

2.1 The Yee Lattice

Finite difference time domain simulation is tasked specifically with simulating Maxwell's curl equations. In order to accomplish this it must discretize on a grid that will yield an accurate result. The Yee grid shown in Figure 3 is the magic

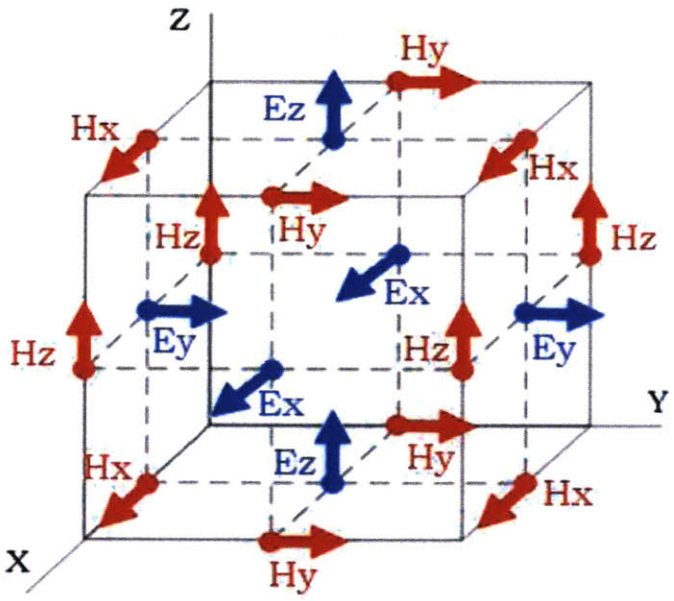

Figure 3: A depiction of the Yee Lattice used to accurately model Maxwell's equations in FDTD simulation whose significance will be discussed in this section. E denotes the electric field and H the magnetic field.

recipe. Later, we will see that finite-difference mode solvers are tasked with discretizing Gauss' law and the wave equation. In the latter case no time

component is required, but in the former time evolution is the crux. Maxwell's six curl equations are given below:

$$\frac{\partial H_x}{\partial t} = \frac{1}{\mu}\left[\frac{\partial E_y}{\partial z} - \frac{\partial E_z}{\partial y} - (M_{source_x} + \sigma^* H_x)\right]$$

$$\frac{\partial H_y}{\partial t} = \frac{1}{\mu}\left[\frac{\partial E_z}{\partial x} - \frac{\partial E_x}{\partial z} - (M_{source_y} + \sigma^* H_y)\right]$$

$$\frac{\partial H_z}{\partial t} = \frac{1}{\mu}\left[\frac{\partial E_x}{\partial y} - \frac{\partial E_y}{\partial x} - (M_{source_z} + \sigma^* H_z)\right]$$

$$\frac{\partial E_x}{\partial t} = \frac{1}{\epsilon}\left[\frac{\partial H_z}{\partial y} - \frac{\partial H_y}{\partial z} - (J_{source_x} + \sigma E_x)\right]$$

$$\frac{\partial E_y}{\partial t} = \frac{1}{\epsilon}\left[\frac{\partial H_x}{\partial z} - \frac{\partial H_z}{\partial x} - (J_{source_y} + \sigma E_y)\right]$$

$$\frac{\partial E_z}{\partial t} = \frac{1}{\epsilon}\left[\frac{\partial H_y}{\partial x} - \frac{\partial H_x}{\partial y} - (J_{source_z} + \sigma E_z)\right]$$

E denotes the electric field and H the magnetic field, σ the electric conductivity and σ^* the equivalent magnetic loss, J_{source} represents an independent current source and M_{source} an independent magnetic source. When examining these equations a couple of things become readily apparent. Consider for example the triplet of field components (Ez, Hy, Hx). In a finite difference scheme with regards to space, if the last curl equation is to be evaluated at a particular spatial point, then both Hy and Hx ought to be located at $\pm \Delta x/2$ or $\pm \Delta y/2$ in order to have consistency. The Yee grid [31], [37] is effectively the invention that takes this into account, allowing an explicit numerical solution to Maxwell's equations that is extremely robust as it can solve for both E and H simultaneously, versus the alternative option of going through the second order wave equation for one component (likely the electric field) and then solving for the other (magnetic field) using the curl equations.

At first the FDTD Yee grid can seem more sophisticated than it actually is. The purpose it tries to accomplish can be overestimated, the impact of that purpose cannot. A simultaneous solution of E and H in a direct way and that does not involve any implicit linear algebra is what has enabled the natural handling of all categories of electromagnetics problems and made FDTD the king of all optical simulation. The next couple of pages are dedicated to displaying the curl equations once they have been discretized on the Yee grid.

The updating field coefficients at the E-field component located at (i, j, k) are given by (using Taflove's & Hagness' notation):

$$C_a|_{i,j,k} = \left(1 - \frac{\sigma_{i,j,k}\Delta t}{2\epsilon_{i,j,k}}\right) / \left(1 + \frac{\sigma_{i,j,k}\Delta t}{2\epsilon_{i,j,k}}\right)$$

$$C_b|_{i,j,k} = \left(\frac{\Delta t}{\epsilon_{i,j,k}\Delta}\right) / \left(1 + \frac{\sigma_{i,j,k}\Delta t}{2\epsilon_{i,j,k}}\right)$$

The updating field coefficients at the H-field component located at (i, j, k) are given by:

$$D_a|_{i,j,k} = \left(1 - \frac{\sigma^*_{i,j,k}\Delta t}{2\mu_{i,j,k}}\right) / \left(1 + \frac{\sigma^*_{i,j,k}\Delta t}{2\mu_{i,j,k}}\right)$$

$$D_b|_{i,j,k} = \left(\frac{\Delta t}{\mu_{i,j,k}\Delta}\right) / \left(1 + \frac{\sigma^*_{i,j,k}\Delta t}{2\mu_{i,j,k}}\right)$$

where Δ is the uniform spatial discretization and Δt is the temporal discretization, ϵ is the permittivity matrix and μ is the permeability matrix, σ is the electric conductivity matrix and σ^* is the equivalent magnetic loss matrix. The discretized curl equations are displayed in the following pages.

$$\mathbf{E_x}|^{n+1/2}_{i,j+1/2,k+1/2} = C_a|_{i,j+1/2,k+1/2}\mathbf{E_x}|^{n-1/2}_{i,j+1/2,k+1/2} + C_b|_{i,j+1/2,k+1/2}\mathbf{H_z}|^{n}_{i,j+1,k+1/2}$$

$$- C_b|_{i,j+1/2,k+1/2}\mathbf{H_z}|^{n}_{i,j,k+1/2} + C_b|_{i,j+1/2,k+1/2}\mathbf{H_y}|^{n}_{i,j+1/2,k}$$

$$- C_b|_{i,j+1/2,k+1/2}\mathbf{H_y}|^{n}_{i,j+1/2,k+1} - C_b|_{i,j+1/2,k+1/2}\mathbf{J_{source_x}}|^{n}_{i,j+1/2,k+1/2}\Delta$$

$$\mathbf{E_y}|^{n+1/2}_{i-1/2,j+1,k+1/2} = C_a|_{i-1/2,j+1,k+1/2}\mathbf{E_y}|^{n-1/2}_{i-1/2,j+1,k+1/2} + C_b|_{i-1/2,j+1,k+1/2}\mathbf{H_x}|^{n}_{i-1/2,j+1,k+1}$$

$$- C_b|_{i-1/2,j+1,k+1/2}\mathbf{H_x}|^{n}_{i-1/2,j+1,k} + C_b|_{i-1/2,j+1,k+1/2}\mathbf{H_z}|^{n}_{i-1,j+1,k+1/2}$$

$$- C_b|_{i-1/2,j+1,k+1/2}\mathbf{H_z}|^{n}_{i,j+1,k+1/2} - C_b|_{i,j+1/2,k+1/2}\mathbf{J_{source_y}}|^{n}_{i-1/2,j+1,k+1/2}\Delta$$

$$\mathbf{E_z}|^{n+1/2}_{i-1/2,j+1/2,k+1} = C_a|_{i-1/2,j+1/2,k+1}\mathbf{E_z}|^{n-1/2}_{i-1/2,j+1/2,k+1/2} + C_b|_{i-1/2,j+1/2,k+1}\mathbf{H_y}|^{n}_{i,j+1/2,k+1}$$

$$- C_b|_{i-1/2,j,k+1}\mathbf{H_y}|^{n}_{i-1,j+1/2,k+1} + C_b|_{i-1/2,j+1/2,k+1}\mathbf{H_x}|^{n}_{i-1/2,j,k+1}$$

$$- C_b|_{i-1/2,j,k+1}\mathbf{H_x}|^{n}_{i-1/2,j+1,k+1} - C_b|_{i-1/2,j,k+1}\mathbf{J_{source_z}}|^{n}_{i-1/2,j+1/2,k+1}\Delta$$

$$\mathbf{H_x}|^{n+1}_{i-1/2,j+1,k+1} = D_a|_{i-1/2,j+1,k+1}\mathbf{H_x}|^{n}_{i-1/2,j+1,k+1} + D_b|_{i-1/2,j+1,k+1}\mathbf{E_y}|^{n+1/2}_{i-1/2,j+1,k+3/2}$$

$$- D_b|_{i-1/2,j+1,k+1}\mathbf{E_y}|^{n+1/2}_{i-1/2,j+1,k+1/2} + D_b|_{i-1/2,j+1,k+1}\mathbf{E_z}|^{n+1/2}_{i-1/2,j+1/2,k+1}$$

$$- D_b|_{i-1/2,j+1,k+1}\mathbf{E_z}|^{n+1/2}_{i-1/2,j+3/2,k+1} - D_b|_{i-1/2,j+1,k+1}\mathbf{M_{source_x}}|^{n+1/2}_{i-1/2,j+1,k+1}\Delta$$

$$\mathbf{H_y}|^{n+1}_{i,j+1/2,k+1} = D_a|_{i,j+1/2,k+1}\mathbf{H_y}|^{n}_{i,j+1/2,k+1} + D_b|_{i,j+1/2,k+1}\mathbf{E_z}|^{n+1/2}_{i+1/2,j+1/2,k+1}$$

$$- D_b|_{i,j+1/2,k+1}\mathbf{E_z}|^{n+1/2}_{i-1/2,j+1/2,k+1} + D_b|_{i,j+1/2,k+1}\mathbf{E_x}|^{n+1/2}_{i,j+1/2,k+1/2}$$

$$- D_b|_{i,j+1/2,k+1}\mathbf{E_x}|^{n+1/2}_{i,j+1/2,k+3/2} - D_b|_{i,j+1/2,k+1}\mathbf{M_{source_y}}|^{n+1/2}_{i,j+1/2,k+1}\Delta$$

$$\mathbf{H_z}|^{n+1}_{i,j+1,k+1/2} = D_a|_{i,j+1,k+1/2}\mathbf{H_z}|^{n}_{i,j+1,k+1/2} + D_b|_{i,j+1,k+1/2}\mathbf{E_x}|^{n+1/2}_{i,j+3/2,k+1/2}$$

$$- D_b|_{i,j+1,k+1/2}\mathbf{E_x}|^{n+1/2}_{i,j+1/2,k+1/2} + D_b|_{i,j+1,k+1/2}\mathbf{E_y}|^{n+1/2}_{i-1/2,j+1,k+1/2}$$

$$- D_b|_{i,j+1,k+1/2}\mathbf{E_y}|^{n+1/2}_{i+1/2,j+1,k+1/2} - D_b|_{i,j+1,k+1/2}\mathbf{M_{source_z}}|^{n+1/2}_{i,j+1,k+1/2}\Delta$$

It is clear from the discretized equations that FDTD is a direct technique. The solutions are always based on field values at previous time steps for all six field components. Because there is no recursion the technique does not involve any linear algebra. This direct nature is brought upon the problem thanks to the Yee grid.

2.2 Computational Complexity of 3D-FDTD

Looking at the Yee grid and the discretized equations in the computational domain provides an interesting segue to analyzing the computational complexity. For one thing, updating the fields at every time step is somewhat local. Since the stencil size is constant we can assume this takes constant time per pixel at every time step. We also see that at every spatial point, the fields need to be updated based on previous field values. This means that we need to store in memory a finite number of values at each point of the computational domain.

Another thing immediately apparent is that FDTD is spatially parallelizable. Once we have the values from all the necessary previous time steps in memory, the new values at each spatial point can be updated in parallel. Again this is because of, and thanks to, the direct nature of the system of equations, and the fact that all field values depend exclusively on stencils from previous values of time.

So far we have seen that the memory required to run FDTD grows with the computational domain, and that FDTD is spatially parallelizable. Note how clear

it is to make these observations just by looking at the discretized curl equations. Understanding the basics of FDTD is really that straightforward, although getting into the details (stability, numerical dispersion, perfectly matched layers and absorbing boundary conditions) can get considerably more complex and is frequently doctoral dissertation material. For the scope of this thesis and in order to understand the value of the hybrid technique this level of indulging in FDTD suffices. The last thing we need to look at is the CPU time and we will be equipped with all the necessary tools.

The number of time steps the algorithm has to run is some fractional power of the volumetric grid cells (N). In our photonic devices as we will later see, there is a forward propagating pulse from the input to the output of the device so that the number of iterations would be $\sim N^{1/3}$ for a cubic simulation domain. At each time step we have to update ~N components. Assuming no spatial parallelization, the total computational burden for large problems is $\sim N^{4/3}$ and decreases as we introduce the level of spatial parallelization to a minimum of $\sim N^{1/3}$. Our TM-FDTD method will push this boundary lower, for a particular device class (assuming *any* available level of spatial parallelizability) and that analysis will be carried out in chapter 5.

We have already discussed that the computational burden of FDTD scales adversely with the number of volumetric grid cells (computational domain size) but that it is spatially parallelizable. This makes the technique highly suited to

advanced computing solutions that employ extreme resources, memory and parallelization such as supercomputers and GPU clusters [38].

This page is intentionally left blank.

Chapter 3

Background on Eigenmode Expansion and Transfer Matrices

3.1 Modal Solutions to Dielectric Waveguide Problems

In the previous section we saw that Maxwell's curl equations can be discretized in time and space to yield a numerical setup for solving electromagnetic propagation *directly*, taking into account E and H. Recall that the wave equation (i.e. $(\nabla^2 + k^2)E = 0$ for an isotropic plane wave) for a particular field (E or H) can be obtained by embedding Gauss' law into the curl equations [39], [40]. For an arbitrary dielectric profile, the wave equation might not have analytical solutions as is elaborated on in Figure 4. In the previous section we bypassed the wave equation and focused exclusively on the dynamics of the curl equations which are responsible for propagation. In this section the spotlight is given to Gauss'

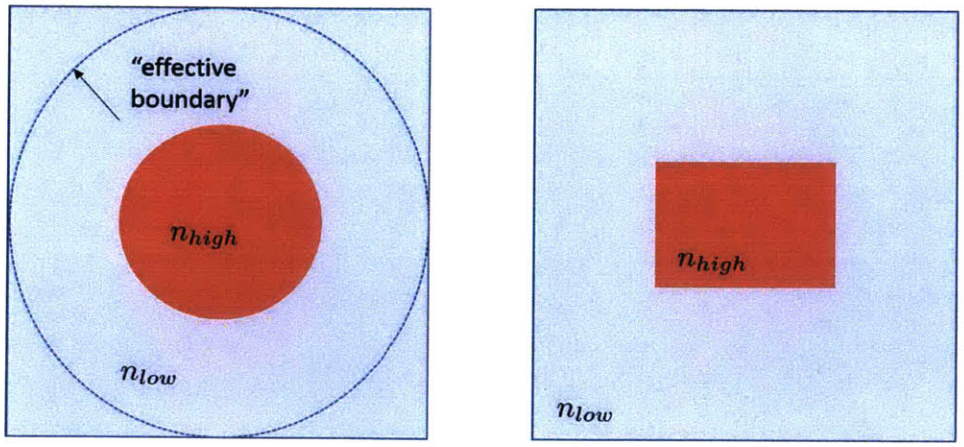

Figure 4: a circular waveguide of high refractive index (left) and a rectangular waveguide (right). The left waveguide adheres to analytical solutions (Bessel functions) but the right does not.

law and the wave equation. In this problem, the temporal and spatial domains are separable, and we care about the latter.

For certain transverse profile dielectric geometries analytical solutions to this wave equation can be obtained. But for silicon on insulator SOI waveguides on a silicon wafer that adhere to rectilinear geometries, a numerical discretization is required. Because the acquisition of modal solutions is vital to Eigenmode Expansion we will cover the math extensively in this section, provide the right intuition and also define the word "modal" as the solution to an eigenvalue problem.

For the problem that will be of interest to us we make the following assumptions. The permittivity is spatially dependent, but isotropic. The permeability is not spatially dependent, but constant isotropic. We assume linear constitutive relationships for the electric displacement and the magnetic flux. The waveguide exhibits no longitudinal variation. This is summed up in the equations below:

- $\mu_x = \mu_y = \mu_z = \mu \neq \mu(x, y, z)$
- $\epsilon_x = \epsilon_y = \epsilon_z = \epsilon(x, y, z)$
- $\bar{D} = \bar{\bar{\epsilon}}\bar{E}$
- $\bar{B} = \bar{\bar{\mu}}\bar{H}$
- $\frac{\partial \epsilon}{\partial z} = 0$

We are interested in obtaining the solution to a dielectric waveguide that exhibits no longitudinal variations, hence the consideration of only the transverse profile. The boundary conditions allow for two kinds of modes, bound and radiation. Bound modes are guided by the core, whereas radiation modes are strictly speaking guided by the boundary of the simulation window. It will be important to keep this distinction in mind. Once the final solution is obtained, only modes whose effective index ($\lambda_0\beta/2\pi$) is greater than the background cladding index will be accepted.

If we denote by ∇_T the transverse component of the Del operator then it can be shown that the transverse and longitudinal wave equations are given by:

$$\left[\nabla_T\left(\frac{1}{\epsilon}\nabla_T\epsilon\ \blacksquare\right)+\nabla_T^2\ +k^2\right]\overline{\mathbf{e}}_{\mathbf{T}}^{\beta}=\beta^2\,\overline{\mathbf{e}}_{\mathbf{T}}^{\beta}$$

$$\mathbf{e}_{\mathbf{z}}^{\beta}=\frac{1}{j\epsilon\beta}\nabla_T\cdot\epsilon\overline{\mathbf{e}}_{\mathbf{T}}^{\beta}=-\frac{j}{\epsilon\beta}\nabla_T\cdot\epsilon\overline{\mathbf{e}}_{\mathbf{T}}^{\beta}$$

Depending on the coordinate system that we are in (Cartesian in our case) these equations can be expanded in different discretizations. This expansion will always reduce to an eigenvalue problem such as the one below:

$$\begin{bmatrix} P_{xx} & P_{xy} \\ P_{yx} & P_{yy} \end{bmatrix} \begin{bmatrix} e_x \\ e_y \end{bmatrix} = \beta^2 \begin{bmatrix} e_x \\ e_y \end{bmatrix} \Leftrightarrow \begin{bmatrix} P_{xx}\mathbf{e_x} + P_{xy}\mathbf{e_y} \\ P_{yx}\mathbf{e_x} + P_{yy}\mathbf{e_y} \end{bmatrix} = \begin{bmatrix} \beta^2\mathbf{e_x} \\ \beta^2\mathbf{e_y} \end{bmatrix} \Leftrightarrow \begin{bmatrix} \mathbf{P}^{\bar{e}^\beta}{}_{:x} \\ \mathbf{P}^{\bar{e}^\beta}{}_{:y} \end{bmatrix}$$

$\overline{\overline{P}}$: **Propagation**

Propagation Constant

Although this is not as critical for Eigenmode Expansion per se, since in our hybrid scheme we will be launching these eigenmodes as sources into FDTD, we desire to discretize on the Yee grid, as is shown in Figure 5 for a small domain.

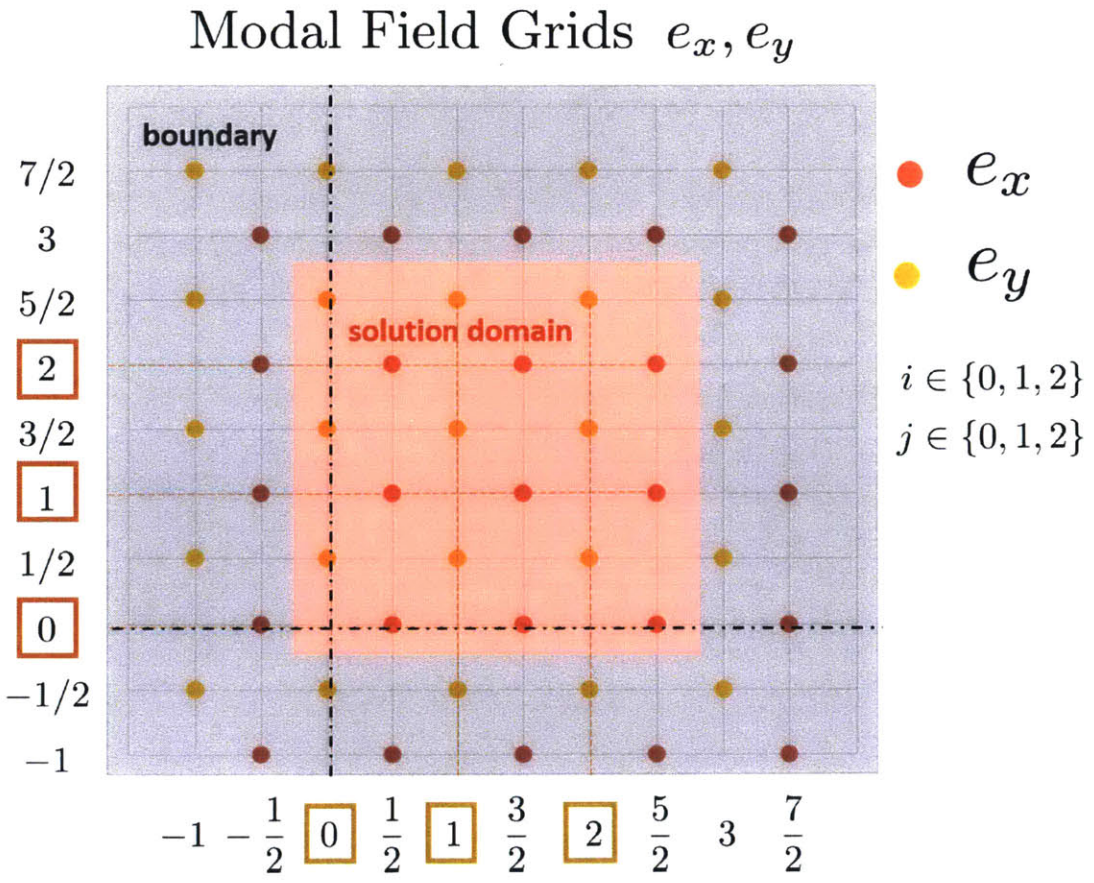

Figure 5: Sample solution domain that we will use as an example in this section and develop the complete eigenvalue matrix for.

The various operators in the propagation matrix are solved for and illustrated below:

$$P_{xx}e_x|_{ij} = \frac{1}{\epsilon_{i+\frac{1}{2},j}}\left[\frac{\epsilon_{i+1,j}e_x|_{i+1,j} - \epsilon_{ij}e_x|_{ij}}{\Delta x^2}\right] - \frac{1}{\epsilon_{i-\frac{1}{2},j}}\left[\frac{\epsilon_{ij}e_x|_{ij} - \epsilon_{i-1,j}e_x|_{i-1,j}}{\Delta x^2}\right] + \frac{e_x|_{i,j+1} - 2e_x|_{ij} + e_x|_{i,j-1}}{\Delta y^2} + \omega^2\mu\epsilon_{ij}e_x|_{ij}$$

$$P_{yy}e_y|_{ij} = \frac{1}{\epsilon_{i,j+\frac{1}{2}}}\left[\frac{\epsilon_{i,j+1}e_y|_{i,j+1} - \epsilon_{ij}e_y|_{ij}}{\Delta y^2}\right] - \frac{1}{\epsilon_{i,j-\frac{1}{2}}}\left[\frac{\epsilon_{ij}e_y|_{ij} - \epsilon_{i,j-1}e_y|_{i,j-1}}{\Delta y^2}\right] + \frac{e_y|_{i+1,j} - 2e_y|_{ij} + e_y|_{i-1,j}}{\Delta x^2} + \omega^2\mu\epsilon_{ij}e_y|_{ij}$$

$$\begin{aligned} P_{xy}e_y|_{ij} = {} & \frac{1}{\epsilon_{i+\frac{1}{2},j}}\frac{\epsilon_{i+\frac{1}{2},j+\frac{1}{2}}e_y|_{i+\frac{1}{2},j+\frac{1}{2}} - \epsilon_{i+\frac{1}{2},j-\frac{1}{2}}e_y|_{i+\frac{1}{2},j-\frac{1}{2}}}{\Delta x\Delta y} \\ & - \frac{1}{\epsilon_{i-\frac{1}{2},j}}\frac{\epsilon_{i-\frac{1}{2},j+\frac{1}{2}}e_y|_{i-\frac{1}{2},j+\frac{1}{2}} - \epsilon_{i-\frac{1}{2},j-\frac{1}{2}}e_y|_{i-\frac{1}{2},j-\frac{1}{2}}}{\Delta x\Delta y} \\ & - \frac{e_y|_{i+\frac{1}{2},j+\frac{1}{2}} - e_y|_{i+\frac{1}{2},j-\frac{1}{2}}}{\Delta x\Delta y} + \frac{e_y|_{i-\frac{1}{2},j+\frac{1}{2}} - e_y|_{i-\frac{1}{2},j-\frac{1}{2}}}{\Delta x\Delta y} \end{aligned}$$

$$\begin{aligned} P_{yx}e_x|_{ij} = {} & \frac{1}{\epsilon_{i,j+\frac{1}{2}}}\frac{\epsilon_{i+\frac{1}{2},j+\frac{1}{2}}e_x|_{i+\frac{1}{2},j+\frac{1}{2}} - \epsilon_{i-\frac{1}{2},j+\frac{1}{2}}e_x|_{i-\frac{1}{2},j+\frac{1}{2}}}{\Delta y\Delta x} \\ & - \frac{1}{\epsilon_{i,j-\frac{1}{2}}}\frac{\epsilon_{i+\frac{1}{2},j-\frac{1}{2}}e_x|_{i+\frac{1}{2},j-\frac{1}{2}} - \epsilon_{i-\frac{1}{2},j-\frac{1}{2}}e_x|_{i-\frac{1}{2},j-\frac{1}{2}}}{\Delta y\Delta x} \\ & - \frac{e_x|_{i+\frac{1}{2},j+\frac{1}{2}} - e_x|_{i-\frac{1}{2},j+\frac{1}{2}}}{\Delta y\Delta x} + \frac{e_x|_{i+\frac{1}{2},j-\frac{1}{2}} - e_x|_{i-\frac{1}{2},j-\frac{1}{2}}}{\Delta y\Delta x} \end{aligned}$$

$$\left\{\begin{array}{rcl} P_{xx}e_x|_{\mathbf{i}+\frac{1}{2},\mathbf{j}} + P_{xy}e_y|_{\mathbf{i}+\frac{1}{2},\mathbf{j}} & = & \beta^2 e_x|_{\mathbf{i}+\frac{1}{2},\mathbf{j}} \\ P_{yx}e_x|_{\mathbf{i},\mathbf{j}+\frac{1}{2}} + P_{yy}e_y|_{\mathbf{i},\mathbf{j}+\frac{1}{2}} & = & \beta^2 e_y|_{\mathbf{i},\mathbf{j}+\frac{1}{2}} \end{array}\right\} \Leftrightarrow \left\{\begin{array}{l} \overline{\overline{\mathbf{P}}} - \beta^2 |\overline{e}_x^{\beta}|_{\mathbf{i}+\frac{1}{2},\mathbf{j}} \\ \overline{\overline{\mathbf{P}}} - \beta^2 |\overline{e}_y^{\beta}|_{\mathbf{i},\mathbf{j}+\frac{1}{2}} \end{array}\right\}$$

Finally, as shown above, the eigenvalue equations need to be evaluated at the proper grid location. In order to construct a sample matrix for the eigenvalue problem and show its structure it behooves us to rank the equations based on the pixel location:

EQUATION 1

$$\begin{array}{ll} \mathbf{1} & \left(\frac{1}{\Delta y^2}\right) e_x|_{i+\frac{1}{2},j-1} \\ \mathbf{2} & \left(\frac{\epsilon_{i-\frac{1}{2},j}}{\epsilon_{ij}} \frac{1}{\Delta x^2}\right) e_x|_{i-\frac{1}{2},j} \\ \mathbf{3} & \left(-\frac{\epsilon_{i+\frac{1}{2},j}}{\epsilon_{i+1,j}} \frac{1}{\Delta x^2} - \frac{\epsilon_{i+\frac{1}{2},j}}{\epsilon_{ij}} \frac{1}{\Delta x^2} - \frac{2}{\Delta y^2} + \omega^2 \mu \epsilon_{i+\frac{1}{2},j}\right) e_x|_{i+\frac{1}{2},j} \\ \mathbf{4} & \left(\frac{\epsilon_{i+\frac{3}{2},j}}{\epsilon_{i+1,j}} \frac{1}{\Delta x^2}\right) e_x|_{i+\frac{3}{2},j} \\ \mathbf{5} & \left(\frac{1}{\Delta y^2}\right) e_x|_{i+\frac{1}{2},j+1} \end{array}$$

EQUATION 1

$$\begin{array}{ll} \mathbf{6} & \left(\frac{\epsilon_{i,j-\frac{1}{2}}}{\epsilon_{ij}} \frac{1}{\Delta x \Delta y} - \frac{1}{\Delta x \Delta y}\right) e_y|_{i,j-\frac{1}{2}} \\ \mathbf{7} & \left(\frac{1}{\Delta x \Delta y} - \frac{\epsilon_{i+1,j-\frac{1}{2}}}{\epsilon_{i+1,j}} \frac{1}{\Delta x \Delta y}\right) e_y|_{i+1,j-\frac{1}{2}} \\ \mathbf{8} & \left(\frac{1}{\Delta x \Delta y} - \frac{\epsilon_{i,j+\frac{1}{2}}}{\epsilon_{ij}} \frac{1}{\Delta x \Delta y}\right) e_y|_{i,j+\frac{1}{2}} \\ \mathbf{9} & \left(\frac{\epsilon_{i+1,j+\frac{1}{2}}}{\epsilon_{i+1,j}} \frac{1}{\Delta x \Delta y} - \frac{1}{\Delta x \Delta y}\right) e_y|_{i+1,j+\frac{1}{2}} \end{array}$$

EQUATION 2

1 $$\left(\frac{\epsilon_{i-\frac{1}{2},j}}{\epsilon_{ij}}\frac{1}{\Delta x\Delta y}-\frac{1}{\Delta x\Delta y}\right)e_x|_{i-\frac{1}{2},j}$$

2 $$\left(\frac{1}{\Delta x\Delta y}-\frac{\epsilon_{i+\frac{1}{2},j}}{\epsilon_{ij}}\frac{1}{\Delta x\Delta y}\right)e_x|_{i+\frac{1}{2},j}$$

3 $$\left(\frac{1}{\Delta x\Delta y}-\frac{\epsilon_{i-\frac{1}{2},j+1}}{\epsilon_{i,j+1}}\frac{1}{\Delta x\Delta y}\right)e_x|_{i-\frac{1}{2},j+1}$$

4 $$\left(\frac{\epsilon_{i+\frac{1}{2},j+1}}{\epsilon_{i,j+1}}\frac{1}{\Delta x\Delta y}-\frac{1}{\Delta x\Delta y}\right)e_x|_{i+\frac{1}{2},j+1}$$

EQUATION 2

5 $$\left(\frac{\epsilon_{i,j-\frac{1}{2}}}{\epsilon_{ij}}\frac{1}{\Delta y^2}\right)e_y|_{i,j-\frac{1}{2}}$$

6 $$\left(\frac{1}{\Delta x^2}\right)e_y|_{i-1,j+\frac{1}{2}}$$

7 $$\left(-\frac{\epsilon_{i,j+\frac{1}{2}}}{\epsilon_{i,j+1}}\frac{1}{\Delta y^2}-\frac{\epsilon_{i,j+\frac{1}{2}}}{\epsilon_{ij}}\frac{1}{\Delta y^2}-\frac{2}{\Delta x^2}+\omega^2\mu\epsilon_{i,j+\frac{1}{2}}\right)e_y|_{i,j+\frac{1}{2}}$$

8 $$\left(\frac{1}{\Delta x^2}\right)e_y|_{i+1,j+\frac{1}{2}}$$

9 $$\left(\frac{\epsilon_{i,j+\frac{3}{2}}}{\epsilon_{i,j+1}}\frac{1}{\Delta y^2}\right)e_y|_{i,j+\frac{3}{2}}$$

Hopefully as we are about to conclude this section, this has made the math substantially more tractable although it does require some time on the part of the reader. Our end goal is now to provide the example of an eigenvalue matrix in order to show the unique sparse block diagonal structure of such a matrix.

$$\overline{\overline{N}} = \begin{bmatrix}
N_{11} & N_{12} & 0 & N_{14} & 0 & 0 & 0 & 0 & 0 & N_{110} & 0 & 0 & N_{113} & 0 & 0 & 0 & 0 & 0 \\
N_{21} & N_{22} & N_{23} & 0 & N_{25} & 0 & 0 & 0 & 0 & 0 & 0 & 0 & N_{213} & 0 & 0 & N_{216} & 0 & 0 \\
0 & N_{32} & N_{33} & 0 & 0 & N_{36} & 0 & 0 & 0 & 0 & 0 & 0 & 0 & 0 & 0 & N_{316} & 0 & 0 \\
N_{41} & 0 & 0 & N_{44} & N_{45} & 0 & N_{47} & 0 & 0 & N_{410} & N_{411} & 0 & N_{413} & N_{414} & 0 & 0 & 0 & 0 \\
0 & N_{52} & 0 & N_{54} & N_{55} & N_{56} & 0 & N_{58} & 0 & 0 & 0 & 0 & N_{513} & N_{514} & 0 & N_{516} & N_{517} & 0 \\
0 & 0 & N_{63} & 0 & N_{65} & N_{66} & 0 & 0 & N_{69} & 0 & 0 & 0 & 0 & 0 & 0 & N_{616} & N_{617} & 0 \\
0 & 0 & 0 & N_{74} & 0 & 0 & N_{77} & N_{78} & 0 & 0 & N_{711} & N_{712} & 0 & N_{714} & N_{715} & 0 & 0 & 0 \\
0 & 0 & 0 & 0 & N_{85} & 0 & N_{87} & N_{88} & N_{89} & 0 & 0 & 0 & 0 & N_{814} & N_{815} & 0 & N_{817} & N_{818} \\
0 & 0 & 0 & 0 & 0 & N_{96} & 0 & N_{98} & N_{99} & 0 & 0 & 0 & 0 & 0 & 0 & 0 & N_{917} & N_{918} \\
N_{101} & 0 & 0 & N_{104} & 0 & 0 & 0 & 0 & 0 & N_{1010} & N_{1011} & 0 & N_{1013} & 0 & 0 & 0 & 0 & 0 \\
0 & 0 & 0 & N_{114} & 0 & 0 & N_{117} & 0 & 0 & N_{1110} & N_{1111} & N_{1112} & 0 & N_{1114} & 0 & 0 & 0 & 0 \\
0 & 0 & 0 & 0 & 0 & 0 & N_{127} & 0 & 0 & 0 & N_{1211} & N_{1212} & 0 & 0 & N_{1215} & 0 & 0 & 0 \\
N_{131} & N_{132} & 0 & N_{134} & N_{135} & 0 & 0 & 0 & 0 & N_{1310} & 0 & 0 & N_{1313} & N_{1314} & 0 & N_{1316} & 0 & 0 \\
0 & 0 & 0 & N_{144} & N_{145} & 0 & N_{147} & N_{148} & 0 & 0 & N_{1411} & 0 & N_{1413} & N_{1414} & N_{1415} & 0 & N_{1417} & 0 \\
0 & 0 & 0 & 0 & 0 & 0 & N_{157} & N_{158} & 0 & 0 & 0 & N_{1512} & 0 & N_{1514} & N_{1515} & 0 & 0 & N_{1518} \\
0 & N_{162} & N_{163} & 0 & N_{165} & N_{166} & 0 & 0 & 0 & 0 & 0 & 0 & N_{1613} & 0 & 0 & N_{1616} & N_{1617} & 0 \\
0 & 0 & 0 & 0 & N_{175} & N_{176} & 0 & N_{178} & N_{179} & 0 & 0 & 0 & 0 & N_{1714} & 0 & N_{1716} & N_{1717} & N_{1718} \\
0 & 0 & 0 & 0 & 0 & 0 & 0 & N_{188} & N_{189} & 0 & 0 & 0 & 0 & 0 & N_{1815} & 0 & N_{1817} & N_{1818}
\end{bmatrix}$$

The above matrix $\overline{\overline{N}}$ shows the structure of the matrix for the eigenvalue problem using perfect electric conductor boundary conditions. The linear system is displayed below:

$$\overline{\overline{N}} \cdot \begin{bmatrix}
e_x|_{\frac{1}{2},0} \\ e_x|_{\frac{3}{2},0} \\ e_x|_{\frac{5}{2},0} \\ e_x|_{\frac{1}{2},1} \\ e_x|_{\frac{3}{2},1} \\ e_x|_{\frac{5}{2},1} \\ e_x|_{\frac{1}{2},2} \\ e_x|_{\frac{3}{2},2} \\ e_x|_{\frac{5}{2},2} \\ e_y|_{0,\frac{1}{2}} \\ e_y|_{0,\frac{3}{2}} \\ e_y|_{0,\frac{5}{2}} \\ e_y|_{1,\frac{1}{2}} \\ e_y|_{1,\frac{3}{2}} \\ e_y|_{1,\frac{5}{2}} \\ e_y|_{2,\frac{1}{2}} \\ e_y|_{2,\frac{3}{2}} \\ e_y|_{2,\frac{5}{2}}
\end{bmatrix} = \beta^2 \cdot \begin{bmatrix}
e_x|_{\frac{1}{2},0} \\ e_x|_{\frac{3}{2},0} \\ e_x|_{\frac{5}{2},0} \\ e_x|_{\frac{1}{2},1} \\ e_x|_{\frac{3}{2},1} \\ e_x|_{\frac{5}{2},1} \\ e_x|_{\frac{1}{2},2} \\ e_x|_{\frac{3}{2},2} \\ e_x|_{\frac{5}{2},2} \\ e_y|_{0,\frac{1}{2}} \\ e_y|_{0,\frac{3}{2}} \\ e_y|_{0,\frac{5}{2}} \\ e_y|_{1,\frac{1}{2}} \\ e_y|_{1,\frac{3}{2}} \\ e_y|_{1,\frac{5}{2}} \\ e_y|_{2,\frac{1}{2}} \\ e_y|_{2,\frac{3}{2}} \\ e_y|_{2,\frac{5}{2}}
\end{bmatrix}$$

The matrix is evidently sparse and can be handled efficiently using sparse linear solvers. An example for a bound optical eigenmode, the eigenvector of a linear system such as the one above we provide Figure 6.

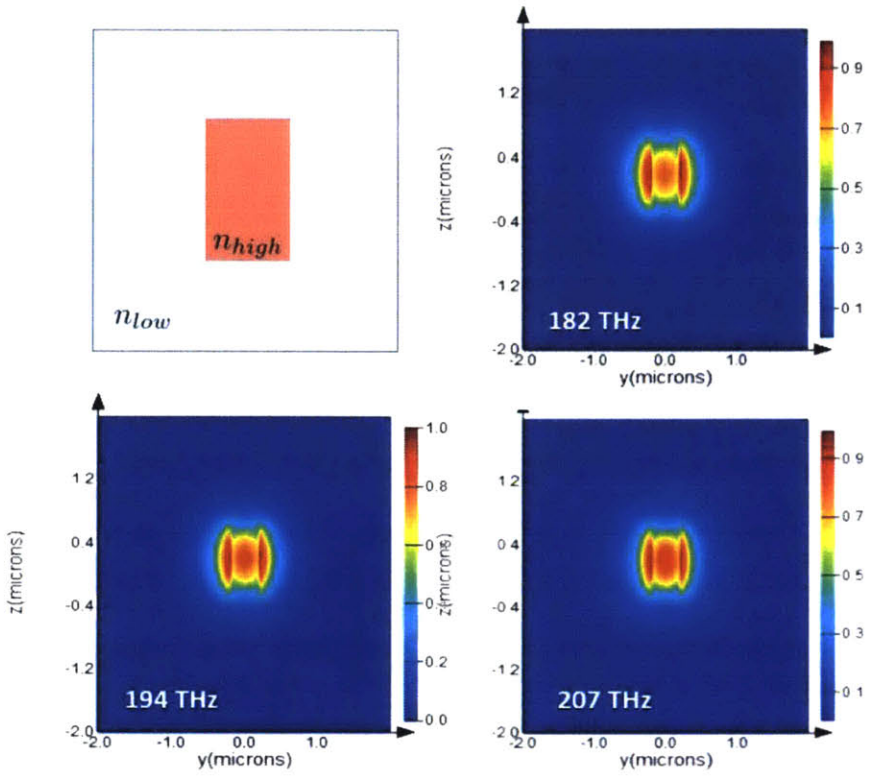

Figure 6: Optical TE eigenmodes of 0.4 x 0.8 um silicon nitride slab waveguide on glass. We observer that as the frequency decreases, the mode expands. Careful considerations must be made for the simulation window to ensure that it contains the bulk of the mode.

3.2 A Vector Space Picture and Transfer Matrices

Once the optical eigenmodes have been acquired numerically they need to be understood in the context of a vector space. Optical waveguide theory suggests

that the electric field distribution at the waveguide cross-section can be decomposed in terms of the eigenmodes [41], [42]. The optical eigenmodes form a complete and orthonormal basis for the vector space in which all transverse field distributions lie:

$$\vec{E}(x,y,z) = \sum_{k=1}^{M} \left(a_k e^{i\beta_k z} + b_k e^{-i\beta_k z}\right) \hat{e}_k(x,y)$$

A similar relationship holds for the magnetic field. If optical eigenmodes are to be viewed as a complete and orthonormal basis, we need to define a dot product relationship:

$$\int \hat{e}_m \times \hat{h}_k^* \cdot d\vec{A} = \delta_{mk}$$

where δ_{mk} is the Dirac delta function that equals 1 when m and k are equal and 0 otherwise. Eigenmode expansion uses tangential boundary conditions on the electric fields at an interface where there is numerically-induced dielectric discontinuity, in conjunction with the orthogonality condition to compute scattering matrices for the device relating all the significant fields [43], [44]. Scattering matrices and transfer matrices that will be of particular interest to us later are equivalent and interchangeable.

This page is intentionally left blank.

Chapter 4

Background on FDTD Speedup Approaches

4.1 The Segmented Finite Difference Time Domain (FDTD) Method

The Segmented FDTD method perhaps bears the most resemblance to the technique developed in this thesis [45]. According to the Segmented FDTD approach, the simulation window is partitioned into linear blocks as shown in Figure 7.

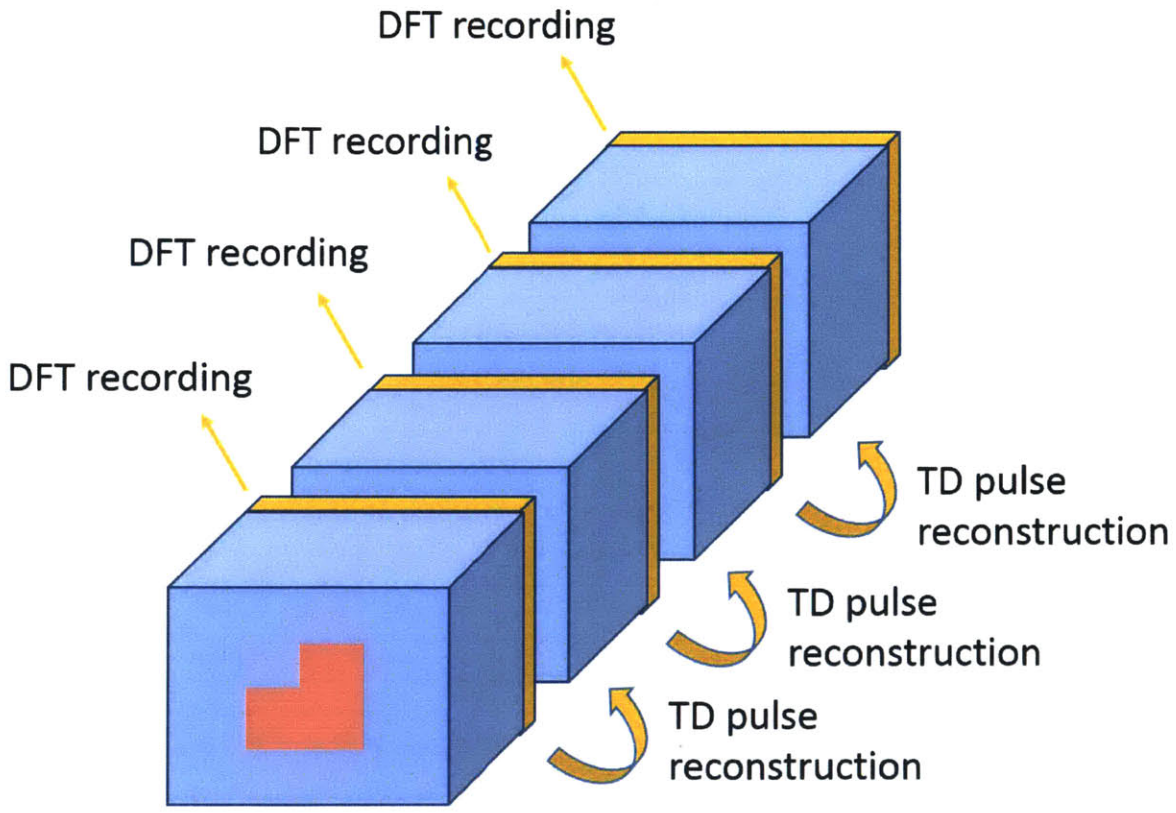

Figure 7: Segmented FDTD diagram and simulation domain partitioning. Discrete Fourier transform (DFT) flux monitors at the end record the information required to completely reconstruct the optical pulse, to be launched in the next simulation etc.

Segmented FDTD then records the Discrete Fourier Transform at the output of each block. By using inverse Fourier techniques it is possible to reconstruct the time domain pulse and seamlessly launch as the input source to the next block. This creates the effect of a net seamless propagation.

Segmented FDTD reduces the CPU time by a factor of 1/K where K is the number of blocks. However, this technique does not provide temporal parallelization as the TM-FDTD method does. In order to simulate the k+1 block we need to wait for the k block to finish.

4.2 Sparse FDTD and Pulse Tracking Approaches

Another popular approach to speed up FDTD with relatively low application specificity consists of implementing a sparse time domain algorithm [18], [46]. As Figure 8 shows, frequently in propagation problems the intensity of light is heavily located.

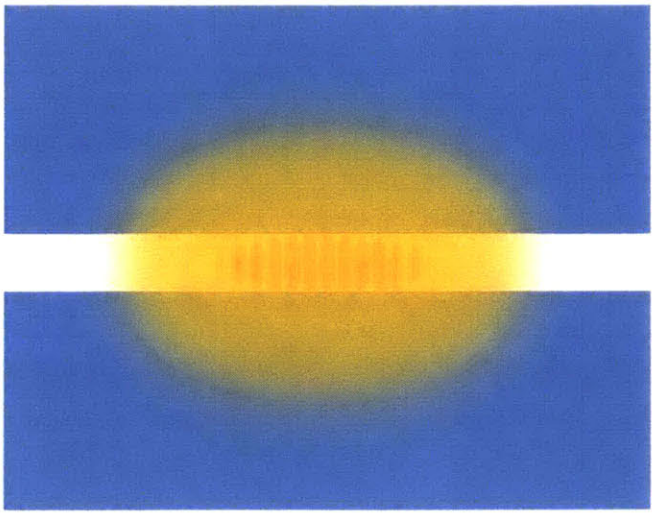

Figure 8: Tracking an optical pulse. Not all points in the simulation domain need to be updated at every time step.

A pulse tracking approach is indeed very insightful and can be automated. But designing specific algorithms requires some intelligence and fine tuning to the problem at hand. The basic concept is to not update the fields at all N volumetric grid cells at every time step, but rather to update only the points that are likely to matter. This can be determined by looking at the previous field value at that particular point. If the optical intensity is above a certain threshold, then update it, if not, then don't bother. As the pulse propagates, the classification of significant and insignificant points shifts as well. At the forward edge of the effective sparse simulation domain, some points will barely make the threshold and get updated. These points now contain a higher field value. It is wise to have the algorithm update a vicinity around those points as well. At the next time step, some other, more forward points will barely make the threshold etc. At the back edge of the effective simulation domain, we have the opposite effect. Some points that got updated will now have a lower value that might not make the threshold and these points will thus get cut in the next updating session.

Note that the above illustration of sparse FDTD describes a scenario that has in mind an optical pulse propagating along a straight waveguide, but it is not difficult to appreciate that there is ample room to extend it to a variety of problems and that many levels of sophistication can be employed in effectively classifying the significant and insignificant points. Interpolation schemes or local low pass filtering may be considered for greater accuracy.

This page is intentionally left blank.

Chapter 5

A Hybrid FDTD-Transfer Matrix Method: (TM-FDTD)

5.1 TM-FDTD Technique Formalization

A typical FDTD simulation consists of propagating an optical pulse within the simulation window as shown in Figure 9. This pulse is typically a spatial eigenmode with a Gaussian temporal envelope centered at some carrier frequency e.g. 193.55 THz for Telecomm. The FDTD code propagates this mode until the light gets absorbed by a perfectly matched layer at the end of the simulation window. By placing flux monitors at the beginning and at the end of the simulation window it is possible to determine the amplitude and phase response of the device over the entire simulation bandwidth through the use of overlap integrals.

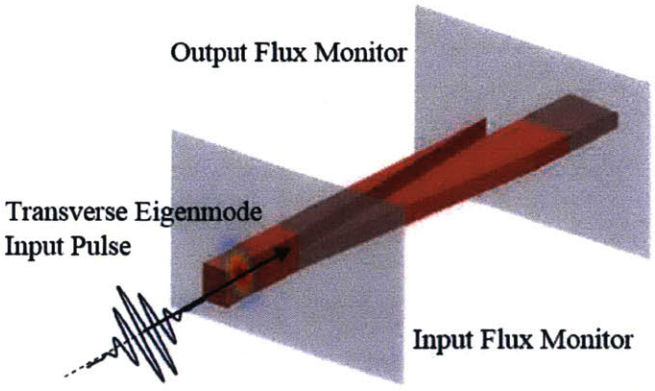

Figure 9: FDTD setup example. Figure previously published by author in [47]

The hybrid TM-FDTD method that we are proposing partitions the simulation window into K blocks of equal dimensions aligned along the propagation axis as shown in Figure 10.

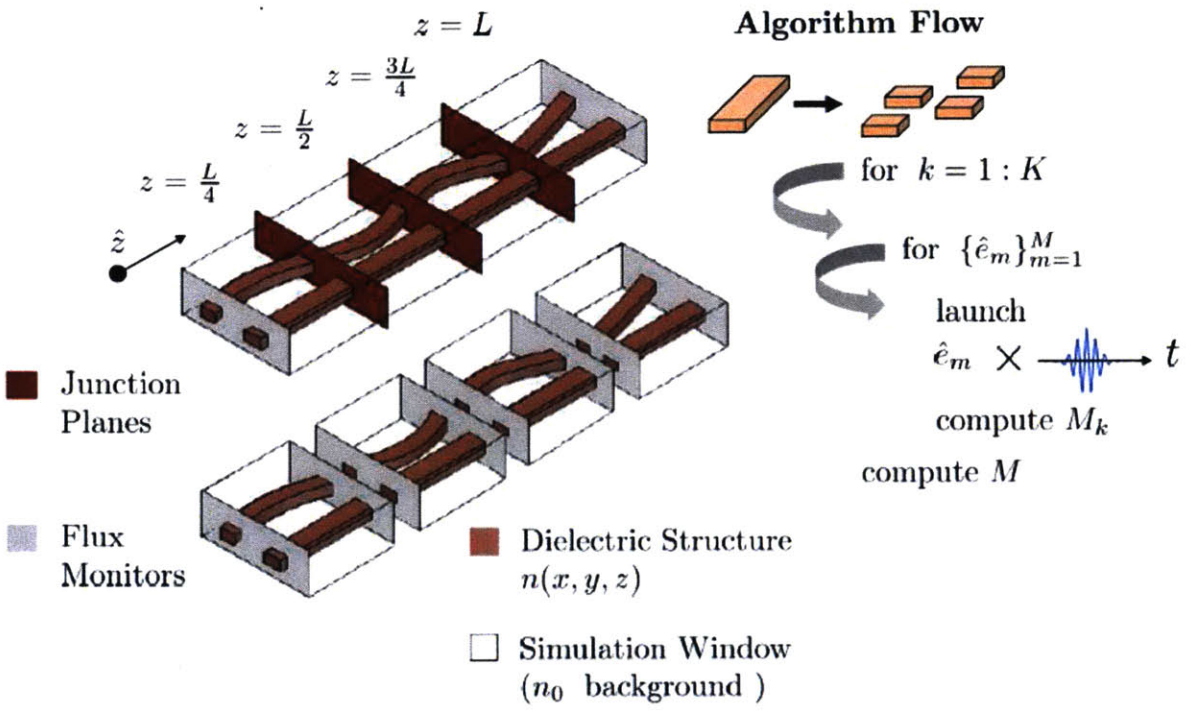

Figure 10: Algorithm flow depicting the hybrid TM-FDTD. The structure displayed here represents some adiabatic photonic structure. The locations where the simulation window gets cut are indicated by the junction planes. M denotes the transfer matrix and $\hat{e}_m$ are the orthonormal eigenmodes.

At every junction using a full vectorial mode solver we obtain the eigenmodes of that cross-section that are necessary to resolve the field distribution in the transverse plane. For every block every front eigenmode is launched into a separate FDTD simulation for that particular block. Under adiabatic assumptions, the eigenmodes suffice to form a complete and orthonormal basis

for resolving the fields at the junctions and are used to decompose the flux monitor content. By obtaining the transfer matrix involving all of the modes for a particular block, we obtain the complete response of that section of the device. The transfer matrices can be multiplied together to yield the complete response for the entire device. Figure 11 shows the most general framework for application of this method. In determining which modes matter, model order reduction techniques can be of high relevance [49].

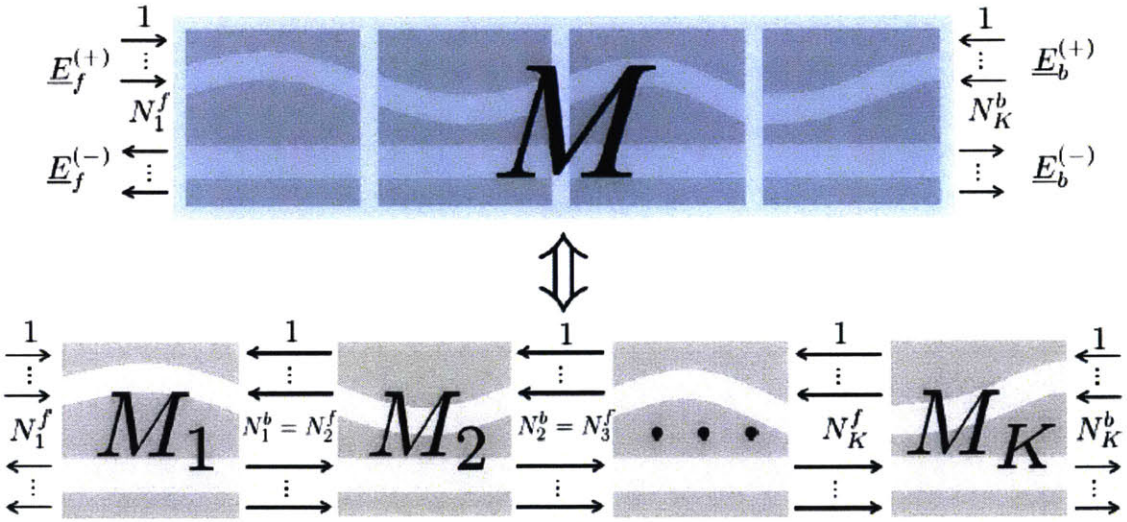

Figure 11: N eigenmodes each forward (+) or backward (-) propagating. Decompositions occur in the $[z_j-\Delta z, z_j+\Delta z]$ longitudinal vicinity of each junction.

At a particular junction there are N eigenmodes each of which could be either forward or backward propagating. Referring to the full device the following equations hold approximately in the longitudinal vicinity of the corresponding junctions:

$$\vec{E}_f^{(sgn)}(x,y,z) = \sum_m a_{f_m}^+ \cdot \hat{e}_{f_m}^{sgn}(x,y)e^{i\alpha_m z}$$
$$\vec{E}_b^{(sgn)}(x,y,z) = \sum_m a_{b_m}^+ \cdot \hat{e}_{b_m}^{sgn}(x,y)e^{i\beta_m z}$$

with a_m, b_m denoting the modal amplitudes. Analogous relations hold for each block individually and at the junction itself we set:

$$U_{f_m}^{(+)} = a_{f_m}^+ e^{i\alpha_m z_j}$$
$$U_{f_m}^{(-)} = a_{f_m}^- e^{i\alpha_m z_j}$$
$$U_{b_m}^{(+)} = a_{b_m}^+ e^{i\beta_m z_j}$$
$$U_{b_m}^{(-)} = a_{b_m}^- e^{i\beta_m z_j}$$

with the U's carrying the amplitude and phase that scales the normalized mode. The eigenmodes $\hat{e}$ are normalized based on the definition of their inner product over the transverse plane. In the context of photonic FDTD simulation, the temporal dependence is given by: $x(t) = G(t)e^{-i\omega_0 t}$ where $G(t)$ is a pulse shape and ω_0 is the carrier frequency. For a particular mode being launched and assuming no reflections for mathematical simplicity (they are very weak in slowly varying devices) we can express the content of the input and output flux monitors as follows:

$$\begin{aligned}\vec{E}_M^{in}(x,y,\omega) &= \hat{e}_{f_m}^{+}(x,y)e^{j\alpha_m z_{start}}X(j\omega) \\ &= U_{f_m}^{(+)}(\omega)\hat{e}_{f_m}^{+}(x,y)\end{aligned}$$

$$\begin{aligned}\vec{E}_M^{out}(x,y,\omega) &= \sum_k a_{b_k}^{+}\hat{e}_{b_k}^{+}(x,y)e^{j\beta_k z_{end}}H(j\omega)X(j\omega) \\ &= \sum_k U_{b_k}^{(+)}(\omega)\hat{e}_{b_k}^{+}(x,y)\end{aligned}$$

with $H(j\omega)$ being the temporal frequency response. The coupling of the launched mode into a particular mode of the back plane can be determined by the ratio of the following overlap integrals:

$$\frac{\int \hat{e}_{b_k}{}^{+}(x,y) \times \left(\vec{H}_M^{out}(x,y)\right)^* \cdot \hat{z}\, dx\, dy}{\int \hat{e}_{f_m}{}^{+}(x,y) \times \left(\vec{H}_M^{in}(x,y)\right)^* \cdot \hat{z}\, dx\, dy} = \frac{U_{b_k}^{(+)}(\omega)}{U_{f_m}^{(+)}(\omega)} = T^{(km)}(\omega)$$

Under the assumption that the vector space spanned by the two lowest order forward propagating modes is sufficient, the device is characterized by the following relation:

$$\begin{bmatrix} U_{b_1}^{(+)} \\ U_{b_2}^{(+)} \end{bmatrix}_\omega = \begin{bmatrix} T^{(11)} & T^{(12)} \\ T^{(21)} & T^{(22)} \end{bmatrix}_\omega \cdot \begin{bmatrix} U_{f_1}^{(+)} \\ U_{f_2}^{(+)} \end{bmatrix}_\omega$$

Typically a transfer matrix will relate both forward and backward propagating waves. For a single mode we would have:

$$\begin{bmatrix} U_{b_1}^{(+)} \\ U_{b_1}^{(-)} \end{bmatrix}_\omega = \begin{bmatrix} M^{(11)} & M^{(12)} \\ M^{(21)} & M^{(22)} \end{bmatrix}_\omega \cdot \begin{bmatrix} U_{f_1}^{(+)} \\ U_{f_1}^{(-)} \end{bmatrix}_\omega$$

where these elements can also be computed from modified overlap integrals. By calculating the overlaps with the reflected modes one obtains a reflection coefficient Γ instead of a transmission coefficient T. The transfer matrix can then be computed as follows:

$$\begin{aligned} M^{(11)} &= T - \Gamma\Gamma'/T' \\ M^{(12)} &= \Gamma'/T' \\ M^{(21)} &= -\Gamma/T' \\ M^{(22)} &= 1/T' \end{aligned}$$

It is now simple to obtain a complete relation between forward and backward propagating waves of multiple modes using a more general transfer matrix. For two modes the complete transfer matrix is given by:

$$\begin{bmatrix} U_{b_1}^{(+)} \\ U_{b_1}^{(-)} \\ U_{b_2}^{(+)} \\ U_{b_2}^{(-)} \end{bmatrix}_\omega = \begin{bmatrix} M_{f_1b_1}^{(11)} & M_{f_1b_1}^{(12)} & M_{f_2b_1}^{(11)} & M_{f_2b_1}^{(12)} \\ M_{f_1b_1}^{(21)} & M_{f_1b_1}^{(22)} & M_{f_2b_1}^{(21)} & M_{f_2b_1}^{(22)} \\ M_{f_1b_2}^{(11)} & M_{f_1b_2}^{(12)} & M_{f_2b_2}^{(11)} & M_{f_2b_2}^{(12)} \\ M_{f_1b_2}^{(21)} & M_{f_1b_2}^{(22)} & M_{f_2b_2}^{(21)} & M_{f_2b_2}^{(22)} \end{bmatrix}_\omega \begin{bmatrix} U_{f_1}^{(+)} \\ U_{f_1}^{(-)} \\ U_{f_2}^{(+)} \\ U_{f_2}^{(-)} \end{bmatrix}_\omega$$

where the superscripts show the analogous element in the single-mode matrix, while the subscripts show the modes involved in the calculation of that element. Finally, the transfer matrix is specific to frequency. The complete transfer matrix is given by a tensor product over all frequencies.

$$M = \otimes_\omega M_\omega = \otimes_\omega (M_{1_\omega} \cdot M_{2_\omega} \cdot \ldots \cdot M_{K_\omega})$$

5.2 Computational Analysis and Experimental Verification

Performing the TM-FDTD method proposed in this thesis yields a clear advantage to regular FDTD. In the 3D-FDTD simulation the CPU runtime scales as $p \cdot n \cdot k_{min}$ where p is the number of grid cells in the transverse dimension, k_{min} is the number of time steps required for the pulse to propagate to the end of the simulation window and n is the number of grid cells along the longitudinal dimension. We will assume for our application that the transverse plane is fixed so that only $n \cdot k_{min}$ is of concern. By assuming a uniform group velocity for the pulse we conclude that $k_{min} \sim n$ which gives us a net scaling of $\sim n^2$ of regular FDTD as applied to this problem.

When K blocks are simulated sequentially our method has a computational scaling of $K \cdot n^2/K^2 \sim n^2/K$, an improvement that is linear in the number of blocks, and quadratic if temporally parallelized. Figures 12 and 13 provide a diagram and results.

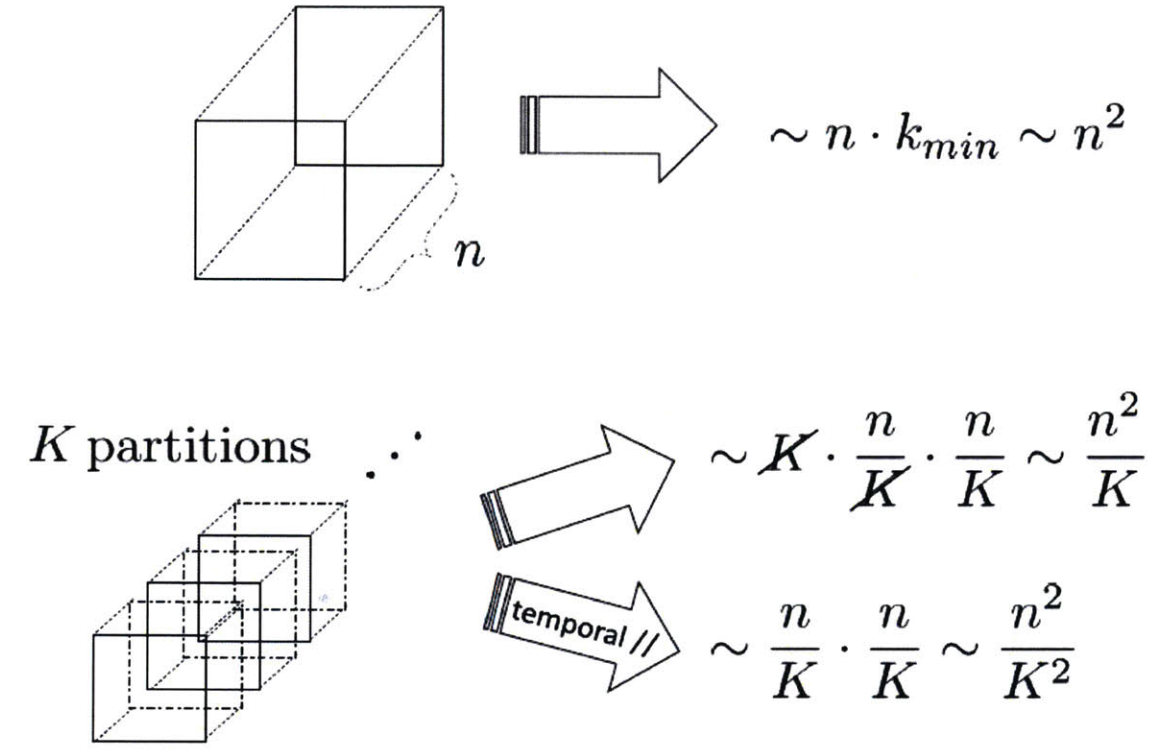

Figure 12: Geometric picture of computational speedup provided by the hybrid TM-FDTD. Overhead due to the computation of the eigenmodes and the overlap integral can be neglected for large devices, and reasonable K making this the correct asymptotic approximation.

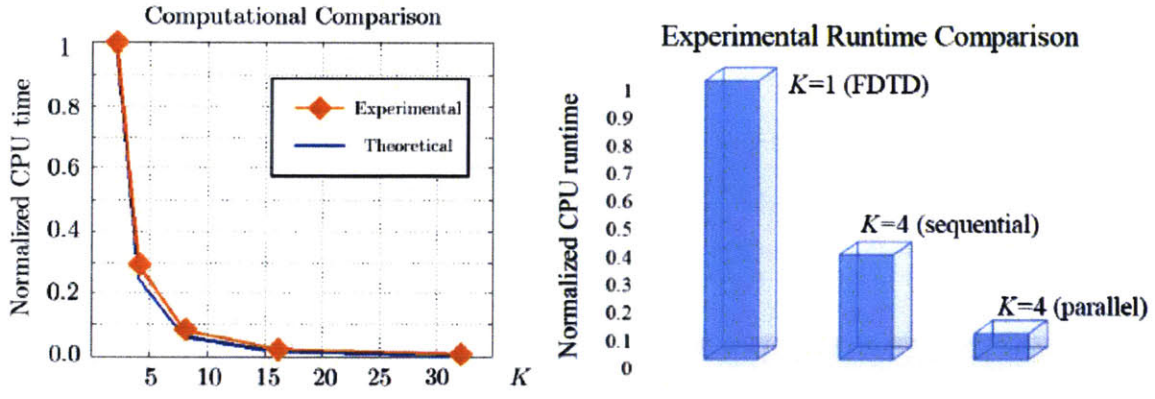

Figure 13: Computational speedup experimental confirmation. The left figure merely serves to match the curve. A simple straight waveguide was used. The right figure presents computational results acquired for an actual polarization rotator of length approximately 17 um.

5.3 Implementation for a Polarization Rotator

We conclude this section of the thesis by presenting the results for the polarization rotator [48] displayed in Figure 14. An impressive accuracy to two significant digits is attained for K=4. A commercial-grade simulator based on the

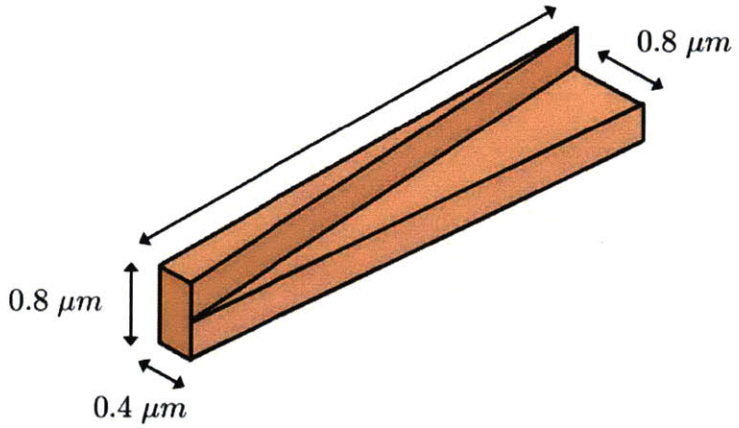

Figure 14: Diagram of device used in simulation.

finite-difference time-domain method [21] was used to verify the results, yielding high confidence for the validity of the technique across "black-box" simulation platforms of which Lumerical is the industry leader. Figures 15-18 contain results that demonstrate the convergence of pure FDTD and TM-FDTD.

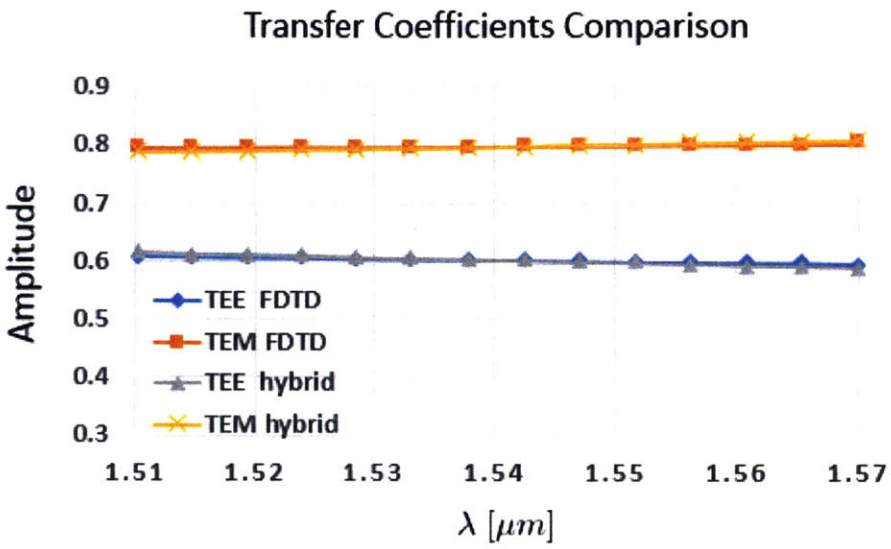

Figure 15: Amplitude coupling coefficients acquired from TE input for a polarization rotator

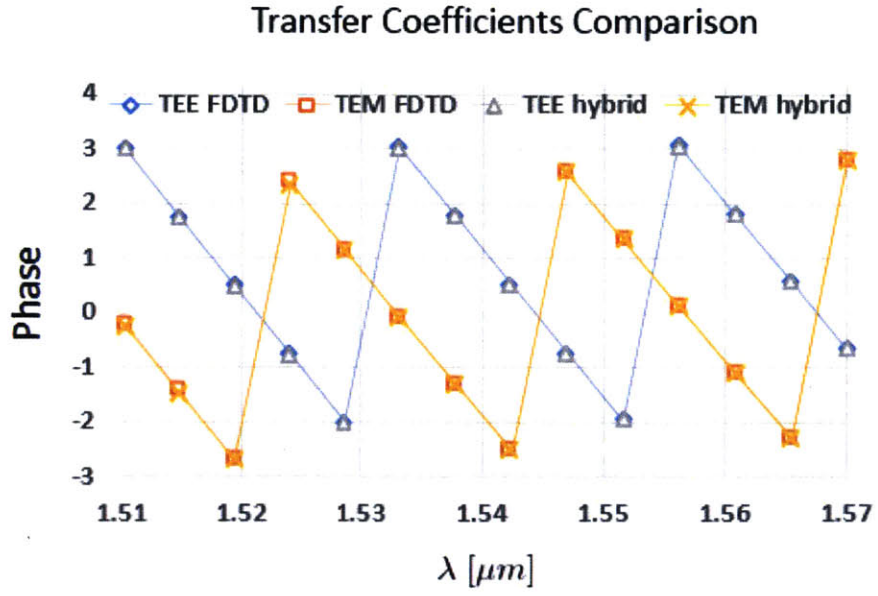

Figure 16: Phase coupling coefficients acquired from TE input for a polarization rotator

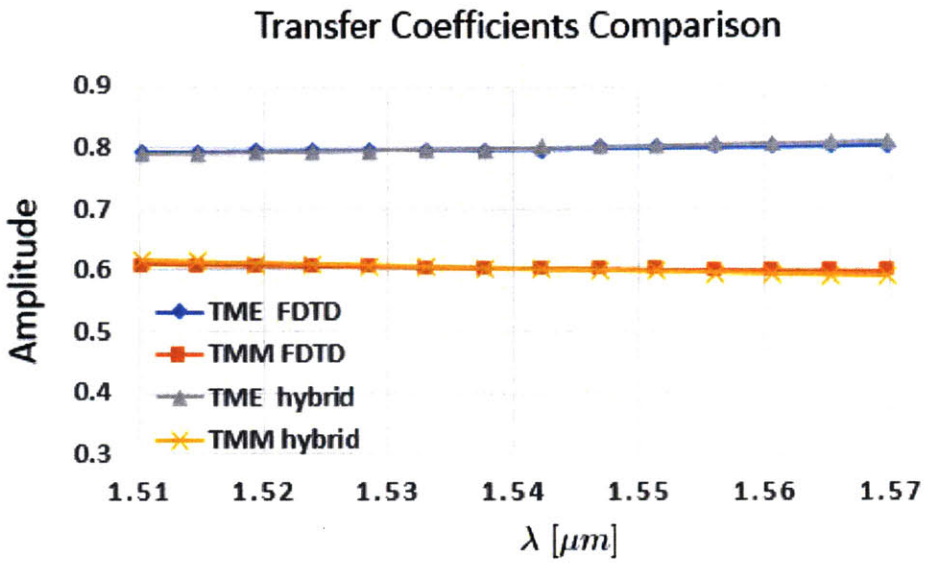

Figure 17: Amplitude coupling coefficients acquired from TM input for a polarization rotator

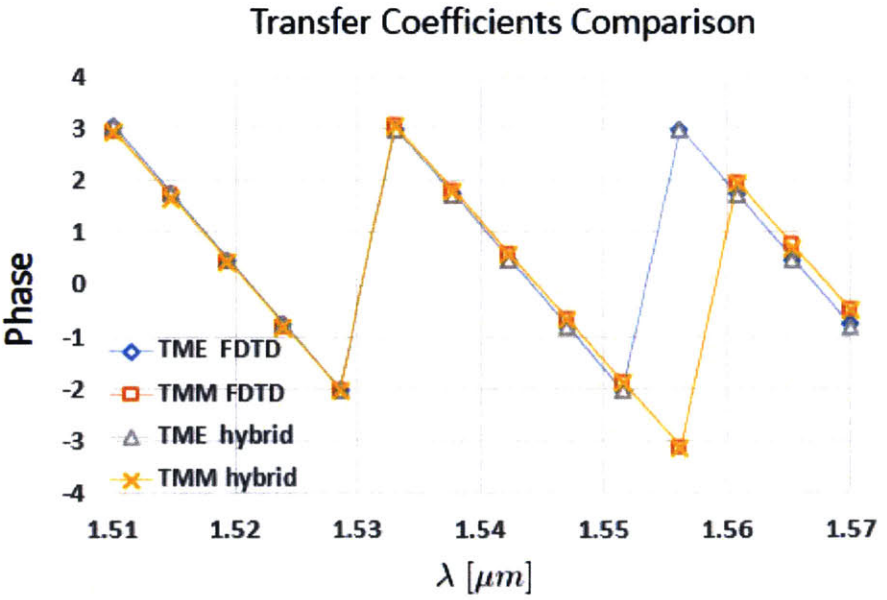

Figure 18: Phase coupling coefficients acquired from TM input for a polarization rotator

This page is intentionally left blank.

Chapter 6

Conclusions

One can always pursue purely modal techniques, and it is unlikely that a time domain technique, let alone FDTD, can outperform the fastest modal technique (where sparseness can be heavily exploited) in terms of CPU runtime. However, the photonics designer has great confidence in 3D FDTD. A 3D FDTD verification of a device serves undoubtedly as the gold standard in the community. As far as eigenmode expansion is concerned there are some even subtler points to be made.

Variants of Eigenmode Expansion make some implicit assumptions about the coupling of the modes, and do not directly solve for it. Because the longitudinal sampling can be relatively large, the boundary conditions the technique applies at the discontinuous interfaces are somewhat artificial. It assumes that overlap integrals between modes of different cross sections are an accurate predictor of the state evolution as the light propagates through that segment. It thus "forces" the transfer matrices. It projects one orthogonal basis onto another orthogonal basis ignoring that the latter is meant to resolve a different vector space. The latter orthogonal basis is actually supposed to be considered in a tensor product space with the former. Our hybrid TM-FDTD technique does exactly that, it respects the tensor product. All overlap integrals are carried out at a particular cross section between the eigenmode expansion monitors and the DFT flux

monitors of that cross section. Two different cross sections are linked only through a complex number division, necessary to yield the correct amplitude (power) and phase for the transfer coefficient, but following a dimensional reduction to 1D and not before. That is thanks to FDTD which comes to fill in the step that EME attempts to skip. The designer could be left wondering if the light would in fact dump some of its power into a component not resolvable by the chosen set of modes. This hypothetical component could not simply be tossed away, although it would be treated like that in Eigenmode Expansion. As this hypothetical component evolves its state, propagating through the device, coupling could be exhibited back into the chosen set of primary eigenmodes so that the power is "returned".

FDTD would handle a case like this quite naturally without a problem and it will always guarantee the correct transfer matrix from the beginning (external input) to the end (final output) of the device. It is true that a hybrid technique such as the one we are proposing also risks losing some of this "spurious power" at the junctions, but handles the remainder of the simulation volume naturally and rigorously and is faster than performing an FDTD simulation for the entire device. Again, we can't have our cake and eat it too! Any simulation technique that attempts to reconcile purely modal and time domain techniques will exhibit the advantages of one and inherent some of the disadvantages of the other. Tradeoffs are inescapable but the trick is to get the best out of both possible worlds and that's what this thesis is all about. This drives the discretization to be exceedingly small, but if the discretization is made too small then it is not at

all hard to end up with an EME simulation setup that is slower than a carefully chosen FDTD setup for the same device.

The segmented FDTD method is similar to our proposition, with the exception that we extend the formalism to suit situations where it is desired to acquire the transfer matrix. More importantly though, our technique introduces temporal parallelizability which is new to an FDTD based technique. But even more importantly, the segmented FDTD method can be combined with our technique to yield even greater speed up. The same holds true for the sparse FDTD.

Finally, future work should involve a thorough error analysis on the one hand as K increase and an exploration of the adiabatic frontier to attempt to extend the range of devices that this technique is applicable to, or, understand why it cannot be extended. We have shown already that it works for short device which are more likely to break the adiabatic limit, but certainly more parameters can be varied here.

In conclusion we have demonstrated, and laid forth the formalism for a hybrid Transfer-Matrix FDTD technique that drastically speeds up simulations in adiabatic photonic devices, is combinable with other techniques, and introduces the concept of temporal parallelization to FDTD.

Bibliography

[1] Ramaswami, R., Sivarajan, K. N., & Sasaki, G. H. (2010). *Optical Networks* (3rd ed.). Burlington, MA, USA: Morgan Kaufmann.

[2] Timurdogan, E., Su, Z., Settaluri, K., Lin, S., Moazeni, S., Sun, C.,...Watts, M. R. (2015). An Ultra Low Power 3D Integrated Intra-Chip Silicon Electronic-Photonic Link. *OFC*.

[3] Watts, M. R. (2005). *Polarization Independent Microphotonic Circuits.* Massachusetts Institute of Technology , Electrical Engineering and Computer Science . Cambridge : MIT.

[4] Su, Z. (2013). *Polarization Manipulation in Silicon Photonics.* Massachusetts Institure of Technology, Electrical Engineering and Computer Science. Cambridge : MIT.

[5] Kimerling, L. C., & Kazumi, W. (Eds.). (2015). *Photonics and Electronics with Germanium* . Weinheim, Germany: Wiley-VCH.

[6] Pond, J., Cone, C., Chrostowski, L., Klein, J., Flueckiger, J., Liu, A.,... Wang, X. (2014). A Complete Design Flow for Silicon Photonics. *SPIE Proceedings: Silicon Photonics and Photonic Integrated Circuits IV, 9133.*

[7] Sun, J., Timurdogan E., Yaacobi A., Hosseini, E.S., Watts, M. R. (2013). Large-scale Nanophotonic Phased Array. *Nature, 493*, 195-199.

[8] Q. Xu, B. S., Xu, Q., Schmidt, B., Pradhan, S., & Lipson, M. (2005). Micrometre-Scale Silicon Electro-Optic Modulator. *Nature, 435*, 325-327.

[9] Reed, G. T. (2008). *Silicon Photonics the State of the Art.* Chichester , England: John Wiley & Sons.

[10] Reed, G. T., & Knights A. P. (2004). *Silicon Photonics An Introduction* . Chichester, England: John Wiley & Sons.

[11] Manolatou, C., Johnson, S. G., Fan, S., Villeneuve, P. R., Haus, H. A., & Joannopoulos, J. D. (1999). High-Density Integrated Optics. *Journal of Lightwave Technology, 17*, 1682-1692.

[12] Chuang, S. L. (2009). *Physics of Photonic Devices* (2nd ed.). Hoboken, NJ, USA: Wiley & Sons.

[13] Beeler, C. (2009, March). All-Optical Computing and All-Optical Networks are Dead. *ACM QUEUE*, pp. 10-11.

[14] Almeida, V. R., Barrios, C. A., Panepucci, R. R., & Lipson, M. (2004). All-Optical Control of Ligh on a Silicon Chip. *Nature, 431*, 1081-1084.

[15] Chen, W., Beck, K. M., Bucker, R., Gullans, M., Lukin, M. D., Suzuki, H. T., & Vuletic, V. (2013). All-Optical Switch and Transistor Gated by One Stored Photon. *Science, 341*, 768-770.

[16] A. Taflove, A. O. (2013). *Advances in FDTD Computational Electrodynamics.* Boston : Artech House.

[17] Ramadan, T. A., Scarmozzino, R., & Osgood, R. M. (1998). Adiabatic Couplers: Design Rules and Optimization. *Journal of Lightwave Technology, 16*, 277-283.

[18] Watts, M. R. (2001). *Wavelength Switching and Routing through Evanescently Induced Absorption.* Massachusetts Institute of Technology, Electrical Engineering and Computer Science. Cambridge: MIT.

[19] Su, Z., Timurdogan, E., Hosseini, E. S., Sun, J., Leake, G., Coolbaugh, D. D., & Watts, M. R. (2014). Four-Port Integrated Polarizing Beam Splitter. *Optics. Lett., 39*, 965-968.

[20] Burr, G. W., & Farjadpour, A. (2005). Balancing Accuracy Against Computation Time: 3-D FDTD for Nanophotonics Device Optimization. *Photonic Crystal Materials and Devices III, 5733.*

[21] Lumerical Solutions, I. (n.d.). http://www.lumerical.com/tcad-products/fdtd/.

[22] Koshiba, M., Tsuji, Y., & Hikari, M. (2000). Time-Domain Beam Propagation Method and Its Application to Photonic Crystal Circuits. *Journal of Lightwave Technology , 18*, 102-110.

[23] Shibayama, J., Muraki, M., Yamauchi, J., & Nakano, H. (2005). Comparative Study of Several Time-Domain Methods for Optical Waveguide Analyses. *Journal of Lightwave Technology, 23*, 2285-2293.

[24] Shibayama, J., Yamahira, A., Mugita T., Yamauchi, J., & Nakano, H. (2003). A Finite-Difference Time-Domain Beam-Propagation Method for TE- and TM-Wave Analyses. *Journal of Lightwave Technology, 21*, 1709-1715.

[25] Inc., P. D. (n.d.). http://www.photond.com/products.htm.

[26] Eleftheriades, G. V., Omar, A. S., Katechi, L. B., & Rebeiz, G. M. (1994). Some Important Properties of Waveguide Junction Generalized Scattering Matrices in the Context of the Mode Matching Technique. *IEEE Trans. on Microwave Theory and Techniques, 42*, 1896-1903.

[27] Haus, H. A. (1984). *Waves and Fields in Optoelectronics.* (N. Holonyak, Ed.) Englewood Cliffs, NJ, USA : Prentice Hall .

[28] Oskooi, A. F., Roundy, D., Ibanescu, M., Bermel P., Joannopoulous, J. D., & Johnson, S. G. (2010). MEEP: A Flexible Free-Software Package for Electromagnetic Simulations by the FDTD Method. *Computer Physics Communications, 181*, 687-702.

[29] D. Gallagher. (2008, February). IEEE LEOS Newsletter. *Industry Research Highlights: Photonics CAD Matures.*

[30] Gallagher, D. F., & Felici, T. P. (2003). Eigenmode Expansion Methods for Simulation of Optical Propagation in Photonics- Pros and Cons. *Proceedings of SPIE Photonics West, 4987*, pp. 69-82. San Jose.

[31] Taflove, A., & Hagness, S. C. (2005). *Computational Electrodynamics* (3rd ed.). Norwood, MA, USA: Artech House.

[32] Moxley III, F. I., Chuss, D. T., & Dai, W. (2013). A Generalized Finite-Difference Time-Domain Scheme for Solving Nonlinear Schrodinger Equations. *Computer Physics Communications, 184*, 1834-1841.

[33] Koos, C., Fujii, M., Poulton, C. G., Steingrueber, R., Leuthold, J., & Freude, W. (2006). FDTD-Modeling of Dispersive Nonlinear Ring Resonators: Accuracy Studies and Experiments. *IEEE Journal of Quantum Electronics, 42*, 1215-1223.

[34] Proakis, J. G., & Manolakis, D. G. (2007). *Digital Signal Processing* (4th ed.). Upper Saddle River, NJ: Prentice Hall .

[35] Yang, F., Chen J., Qiang, R., & Eisherbeni, A. (2007). A Simple and Efficient FDTD/PBC Algorithm for Scattering Analysis of Periodic Structures. *Radio Science, 42.*

[36] Petracek, J., & Luksch, J. (2011). Bidirectional Eigenmode Propagation Algorithm for 3D Waveguide Structures. *ICTON.*

[37] Yee, K. S. (1966). Numerical Solution of Initial Boundary Value Problems Involving Maxwell's Equations in Isotropic Media . *IEEE Trans. Antennas and Propagation* , (pp. 302-307).

[38] Yu, W., Yang, X., Liu, Y., Mittra, R., & Muto, A. (2011). *Advanced FDTD Methods.* Norwood, MA, USA: Artech House.

[39] Born, M., & Wolf, E. (1999). *Principles of Optics* (7th ed.). New York, NY, USA: Cambridge University Press.

[40] Kong, J. A. (2000). *Electromagnetic Wave Theory.* Cambridge , MA, USA: EMW Publishing .

[41] Snyder, A. W., & Love, J. D. (1983). *Optical Waveguide Theory.* London , UK: Kluwer Academic Publishers.

[42] Okamoto, K. (2006). *Fundamentals of Optical Waveguides* (2nd ed.). Burlington , MA, USA: Academic Press.

[43] Teich, M. C., & Saleh, B. A. (2007). *Fundamentals of Photonics.* Hoboken, NJ, USA: John Wiley & Sons.

[44] Rumpf, R. C. (2011). Improved Formulation of Scattering Matrices for Semi-Analytical Methods that is Consistent wtih Convention. *Progress In Electromagnetics Research B, 35*, 241-261.

[45] Wu, Y., & Wassell, I. (2009). Introduction to the Segmented Finite-Difference Time-Domain Method. *IEEE Trans. on Magnetics, 45*, pp. 1364-1367.

[46] Doerr, C. R. (2013). Sparse Finite Difference Time Domain Method. *IEEE Phot. Tech. Lett., 25*, 2259-2262.

[47] Samolis, C. D., & Daniel, L. (2015). A Hybrid FDTD-Transfer Matrix Method Applicable to Adiabatic Photonic Simulation. *The 31st International Review of Progress in Applied Compuational Electromagnetics.* Williamsburg, VA.

[48] Watts, M. R., & Haus, H. A. (2005). Integrated Mode-Evolution-Based Polarization Rotators. *Optics Lett., 30*, 138-140.

[49] Antoulas, A. C., Sorensen, D. C., & Gugercin, S. (2001). A survey of model reduction methods for large-scale systems. *Contemporary mathematics, 280*, 193-220.

[50] Deinega, A., Belousov, S., & Valuev, I. (2009). Hybrid Transfer-Matrix FDTD Method for Layered Periodic Structures. *Optics Letters, 34*, 860-862.

[51] Deingea, A., Belousov, S., & Valuev, I. (2013). Transfer-Matrix Approach for Finite-Difference Time-Domain Simulation of Periodic Structures. *Physical Review E, 88.*

[52] Oppenheim, A. V., Wilsky, A. S., & Nawab, H. S. (1983). *Signals and Systems* (2nd ed.). Upper Saddle River, NJ, USA: Prentice Hall.

[53] Inan, U. S., & Marshall, R. A. (2011). *Numerical Electromagnetics.* Cambridge , UK: Cambridge University Press .

[54] Bai, N., Feng, J., Liao, F., & Sun, X. (2013). Fast Analysis for Electromagnetic Band Gap Waveguides Using Compact Finite-Difference-Time-Domain Method. *AEU - International Journal of Electronics and Communications, 67*, 1025-1029.

[55] Sudbo, A. S. (1993). Film mode matching: a versatile numerical method for vector mode field calculation in dielectric waveguides. *Pure Appl. Opt., 2*, 211-233.

[56] Sullivan, D. M. (2000). *Electromagnetic Simulation Using the FDTD Method.* (R. D. Booton, Ed.) New York , NY, USA : IEEE Press .

[57] Yariv, A., & Yeh, P. (2007). *Photonics Optical Electronics In Modern Communications* (6th ed.). New York, NY, USA: Oxford University Press.